






# Modeling of stress corrosion cracking growth rates for key structural materials of nuclear power plant

Zhenhua Li<sup>1</sup> , Yonghao Lu<sup>1,\*</sup> , and Xinyu Wang<sup>1</sup> 

<sup>1</sup>National Center for Materials Service Safety, University of Science and Technology Beijing, Beijing 100083, China

**Received:** 28 May 2019

**Accepted:** 22 August 2019

**Published online:**  
6 September 2019

© Springer Science+Business Media, LLC, part of Springer Nature 2019

## ABSTRACT

Stress corrosion cracking in light water reactor is one of the most important factors threatening the safe operation of nuclear power plants. Due to the severity, generality and various safety and economic problems caused by this phenomenon, it is necessary to establish a model for predicting the stress corrosion cracking growth rates. This paper provides an overview of three main methods for predicting stress corrosion cracking growth rates in recent decades, i.e., empirical, deterministic and calculation methods, which are introduced in detail. Empirical models describe classical statistical analysis and emerging artificial neural network method, both of which are based on a large number of experimental test data mining. They are convenient and relatively accurate in predicting, but require extensive, time-consuming and expensive tests for different service environments. Deterministic models aim to establish a theoretical relationship between crack growth rate and various influencing parameters by studying the stress corrosion cracking mechanism. Many scholars have proposed different mechanisms to scientifically explain the stress corrosion cracking phenomenon and propose corresponding crack growth rate models. Calculation models reveal the mechanism of crack initiation and propagation in different layers of materials by means of finite element method based on fracture mechanics and multiscale method based on quantum mechanics. They provide new idea for future research on stress corrosion cracking and bridge the quantitative mechanism or model, but no specific stress corrosion cracking growth rate model is formed. The article concludes with the prospect, aim and direction for stress corrosion cracking mechanism and prediction model.

Address correspondence to E-mail: lu\_yonghao@mater.ustb.edu.cn

## Introduction

The long-term operation experience of advanced nuclear power countries in the world indicates that stress corrosion cracking (SCC), as a representative of environmentally assisted cracking (EAC), has become one of the main reasons for the failure of light water reactor (LWR) components [1, 2]. SCC often causes long-term and costly shutdowns and repairs and even safety problems such as nuclear radiation leakage, which has become one of the main problems affecting the economic and safety of the entire system operation. Therefore, it is particularly important to study the mechanism of SCC, especially to predict the SCC growth rates [3–5].

Therefore, scientists all over the world are striving to establish a model that can accurately predict the SCC growth rates for key structural materials of nuclear power plant [6–10]. However, SCC is an extremely complex phenomenon, and there are more than 20 known factors, which makes it very difficult to establish this model. When predicting phenomena in physics or engineering, there are usually two basic philosophical perspectives: empirical and deterministic. Empirical means that to know something, one must experience it first, while the deterministic view holds that the basis of the past (such as some laws of nature) can be used to predict the form of the future. But no matter which viewpoint is based on, in order to predict future corrosion evolution based on the current stress corrosion state, it is necessary to clarify the important role of independent variables (such as temperature, stress intensity, conductivity) in predicting variables (such as crack growth rate (CGR)).

At present, the general models for predicting SCC growth rates in the world are roughly divided into three categories: one is an empirical prediction model based on a large number of experimental data and field data, the other is a deterministic prediction model based on various SCC mechanisms and the third is a prediction model combining calculation and simulation with SCC mechanism. The establishment of relevant prediction models can guarantee the safe, efficient and economical operation of nuclear power plants, and the accurate CGR calculation model can provide theoretical guidance for the maintenance and replacement of related components of nuclear power plants, minimizing the interruption of power generation caused by accidents, and can reduce the occurrence of leakage accidents due to crack damage,

which are the significance and practical application of establishing a SCC growth rates prediction model [11, 12].

## Empirical prediction models based on data mining

The empirical prediction model is a prediction model based on laboratory data and field data. At present, there are many types of prediction methods, from classical statistical analysis to current gray prediction, expert system and fuzzy mathematics, and even the emerging neural networks method. SCC has been proven to be a highly complicated process in which materials, environment and stress work together. By screening and identifying various influencing factors as input variables and taking the objects to be studied as output variables, the empirical prediction models will provide a new approach for the study of SCC growth rates.

## Materials Reliability Program model

The Materials Reliability Program (MRP) model refers to the CGR curves obtained by the Electric Power Research Institute (EPRI) based on a statistical analysis of the worldwide set of available laboratory test data. In the report MRP-55 [13], MRP proposed a CGR disposition curve for primary water stress corrosion cracking (PWSCC) of thick-wall alloy 600 material, which was also reported by White et al. [14]. The CGR model proposed by MRP-55 is mainly carried out in two steps. The first step in establishing the CGR curve of alloy 600 is to determine the form of CGR dependence on stress intensity factor (SIF). The second step is to consider the variability of CGR due to the differences in thermomechanical material processing and microstructure. MRP also proposed a CGR disposition curve for PWSCC of alloy 182/132 and 82 welds in the report MRP-115 [15], which was also reported by White et al. [16]. The MRP-115 curve contains the effects of SIF, temperature and thermal activation energy as well as welds orientation [17]. With the extensive application of alloy 690 and its welding metals in new pressurized water reactor (PWR), MRP recently proposed CGR models for PWSCC of alloy 690 and alloys 52, 152, and variants welds in the report MRP-386 [18]. EPRI has compiled databases of more than 500 alloy 690 CGR data points

and 130 alloy 52/152 CGR data points by using thick-walled compact tensile (CT) specimens from seven research laboratories. The data quality is scored and evaluated to determine the effects of temperature, yield strength, crack tip SIF and crack orientation. MRP updated the CGR model for PWSCC of alloy 600 in the report MRP-420 and explained the threshold of SIF [19].

For the continued safe operation of nuclear power plants, Scott first established a CGR model for PWSCC of alloy 600 materials as a function of SIF, which was derived from published laboratory data [20]:

$$\frac{da}{dt} = C \cdot (K - 9)^{1.16} \tag{1}$$

where  $K$  is the SIF, in which the threshold value is 9 MPa m<sup>2</sup>.  $C$  is the correction coefficient, and the value of  $C$  corresponds to different temperatures.  $da/dt$  is the CGR, which can also be denoted by  $\dot{a}$ .

The CGR model proposed by MRP-55 adopts the SIF dependence form of Scott equation and also uses Scott’s value for the exponent  $\beta_1$  (1.16) rather than letting the exponent be determined by the statistics. Moreover, the effect of different temperatures on the CGR is explained by introducing Arrhenius equation for thermally controlled processes. The general formal equation obtained from MRP-55 is as follows:

$$\frac{da}{dt} = \exp\left[\frac{-Q_g}{R}\left(\frac{1}{T} - \frac{1}{T_{ref}}\right)\right] \alpha_1 (K - K_{th})^{\beta_1} \tag{2}$$

where  $Q_g$  is the thermal activation energy for crack growth (130 kJ/mol),  $R$  is the universal gas constant (8.314 × 10<sup>-3</sup> kJ mol<sup>-1</sup> K),  $T$  is the absolute operating temperature at location of crack,  $T_{ref}$  is the reference temperature corresponding to the normalized data (598.15 K),  $\alpha_1$  is the power-law constant ( $\alpha_1 = 2.67 \times 10^{-12}$  at 325 °C),  $K_{th}$  is the threshold crack tip SIF,  $\beta_1$  is the power-law exponent, and the value is 1.16.

The statistical method for establishing the CGR equation by MRP115 is similar to that proposed for the alloy 600 wrought material in MRP-55, but includes a linearized multiple regression model to determine a best fit SIF exponent  $\beta_2$  while still processing data heat-by-heat. The MRP database indicates that the CGR for alloy 82 is on average 2.6 times lower than that for alloy 182/132, so the MRP-115 curve for alloy 82 is 2.6 times lower than the curve for

alloy 182/132 [15]. The general form of the MRP-115 equation for alloy 182/132 and alloy 82 is as follows:

$$\frac{da}{dt} = \exp\left[\frac{-Q_g}{R}\left(\frac{1}{T} - \frac{1}{T_{ref}}\right)\right] \alpha_2 f_{alloy} f_{orient} K^{\beta_2} \tag{3}$$

where  $f_{alloy} = 1.0$  for alloy 182 or 132 and  $1/2.6 = 0.385$  for alloy 82,  $f_{orient} = 1.0$  except 0.5 for crack propagation that is clearly perpendicular to the dendrite solidification direction,  $\alpha_2$  is the power-law constant ( $\alpha_2 = 1.5 \times 10^{-12}$  at 325 °C),  $\beta_2$  is the power-law exponent, and the value is 1.6.

The basic form of the alloy 690 and alloy 52/152 models is similar to the MRP-55 and MRP-115 disposition equations for alloy 600 and alloy 82/182, respectively. Several new terms have been added to alloy 690 model (such as hydrogen concentration, yield strength and receiving heat treatment state) to better reflect more testing materials and environments and to improve understanding of the effects of these variables [21]. The general form of alloy 690 CGR model is as follows, and each parameter is explained:

$$\frac{da}{dt} = \alpha_3 \cdot f_K \cdot f_T \cdot f_{H_2} \cdot f_{YS} \cdot f_{HT} \cdot f_{orient} \cdot f_{product\ form} \cdot f_{ARcond} \tag{4}$$

$$f_K = K^{\beta_3} \tag{5}$$

where  $\alpha_3$  is the power-law constant ( $\alpha_3 = 4.5 \times 10^{-17}$  at 325 °C),  $f_K$  is the factor accounting for crack tip stress intensity factor in MPa m<sup>2</sup>,  $\beta_3$  is the power-law exponent, and the value is 2.5,  $f_T$  is the factor adjusting CGR to a common reference temperature in °C,  $f_{H_2}$  is the factor accounting for dissolved hydrogen concentration in relation to the Ni/NiO transition in cc/kg H<sub>2</sub> at STP,  $f_{YS}$  is the factor adjusting CGR to a common yield strength in MPa,  $f_{HT}$  is the factor accounting for heat treatment of laboratory application,  $f_{orient}$  is the factor explaining the difference in CGR caused by crack growth in certain direction,  $f_{product\ form}$  is the factor explaining the difference in CGR produced by samples processed from different product forms and  $f_{ARcond}$  is the factor explaining the CGR difference caused by the material state obtained by mill annealed or thermally treated.

EPRI has done a lot of test data collection and evaluation work for the service safety of nuclear power structural materials that can be directly applied to crack assessment calculations for plant

components and continuously updates and improves the CGR model, which plays a crucial role in the safe operation of nuclear power plant. The CGR curve proposed by MRP can be regarded as the average value of the upper half part of the discrete distribution of different CGR data corresponding to different grades of material. Therefore, the MRP curve addresses the concern that heats that are more susceptible than average to crack initiation tend to have higher CGRs. Cracking detected in the operating nuclear power plants would tend to be located in components fabricated from such susceptible heats. However, the MRP model is based on the fitting of laboratory data, which requires a large number of time-consuming and expensive tests for different service environments and specific nuclear power materials. It only considers input and output, but has nothing to do with process mechanism.

### Artificial neural network model

Artificial neural networks (ANNs) are nonlinear science that imitate the structure and intelligence of human brain. With their unique self-organization, self-learning, fast processing, high fault tolerance and strong nonlinear function approximation ability, ANNs have become a powerful tool for dealing with nonlinear systems. The trained neural network can simulate the relationship between variables of complex system and then help people to analyze the intrinsic mechanism of complex system. ANNs have been successfully applied by a number of researchers in the field of corrosion prediction. Smets and Bogaerts [22] successfully applied ANNs to SCC risk prediction of austenitic stainless steels and analyzed the combined effects of temperature, chloride concentration and oxygen content on the occurrence of SCC in high-temperature water. Lu et al. [23] first applied ANNs to predict SCC growth rate, in which they applied ANNs to study the intergranular stress corrosion cracking (IGSCC) in sensitized 304 stainless steel in high-temperature aqueous solutions. Kamrunnahr and Urquidi-Macdonald [24, 25] used ANNs as data mining tools to predict the corrosion behavior of metal alloys, which was helpful to classify and sort some parameters, and to understand the synergistic effects of parameters and variables on electrochemical potential and corrosion rate. Shi et al. [26, 27] established the database of CGR of 304 stainless steel and alloy 600 IGSCC in LWR

environment and the corresponding ANN model, which indicated that the ANN model could predict the effect of various variables on CGR. Halama et al. [28], Li et al. [29] and Hu et al. [30] used ANN model to study the corrosion phenomenon of metal alloys in different environments, respectively. Therefore, for complex systems that are difficult to accurately predict by mathematical models, ANNs provide a new solution which can make accurate predictions by learning from existing data.

ANNs can be divided into many different types according to the difference of neural network structure and learning algorithm, among which the back-propagation feed-forward neural network (BPNN) learning is the most widely used [31–33]. A typical three-layer neural network structure is shown in Fig. 1a; the first layer (also known as input layer) receives input signals from the external environment and transmits them to the neurons connected to the next layer. The last layer (called the output layer) is used to output the results we need. The layer between the input layer and the output layer is called the hidden layer, which is the internal processing layer of the neural network. For complex nonlinear system simulation, using more hidden layers can make the system more stable [34]. Each layer contains one or more neurons, and the model is shown in Fig. 1b. It has three basic elements: a set of connections (corresponding to synapses of biological neurons), and the connection strength is represented by the weights on each of the connections, which are positive for activation and negative for inhibition; a summation unit  $\sum$  which is used to calculate the weighted sum of each input signals; and an activation function  $f$ , which is used for mapping, and the output amplitude of neurons is limited to a certain range.

Mathematically, the output of the  $k$ th neuron in the  $l$ th layer receiving a  $n$ -dimensional input vector is [35]:

$$y_k^{(l)} = f \left( b_k^{(l)} + \sum_{i=1}^n w_{k,i}^{(l)} x_i^{(l)} \right) \quad (6)$$

where  $y_k$  is the response of the  $k$ th neuron to an input vector  $x = (x_1, x_2, \dots, x_n)$  and  $x_i$  represents the input parameters.  $w_{k,i}$  are the weights that are used to scale the respective input value to the neuron.  $b_k$  is called the bias that is used to account for the contribution of the unknown but influential parameters that have been left out.

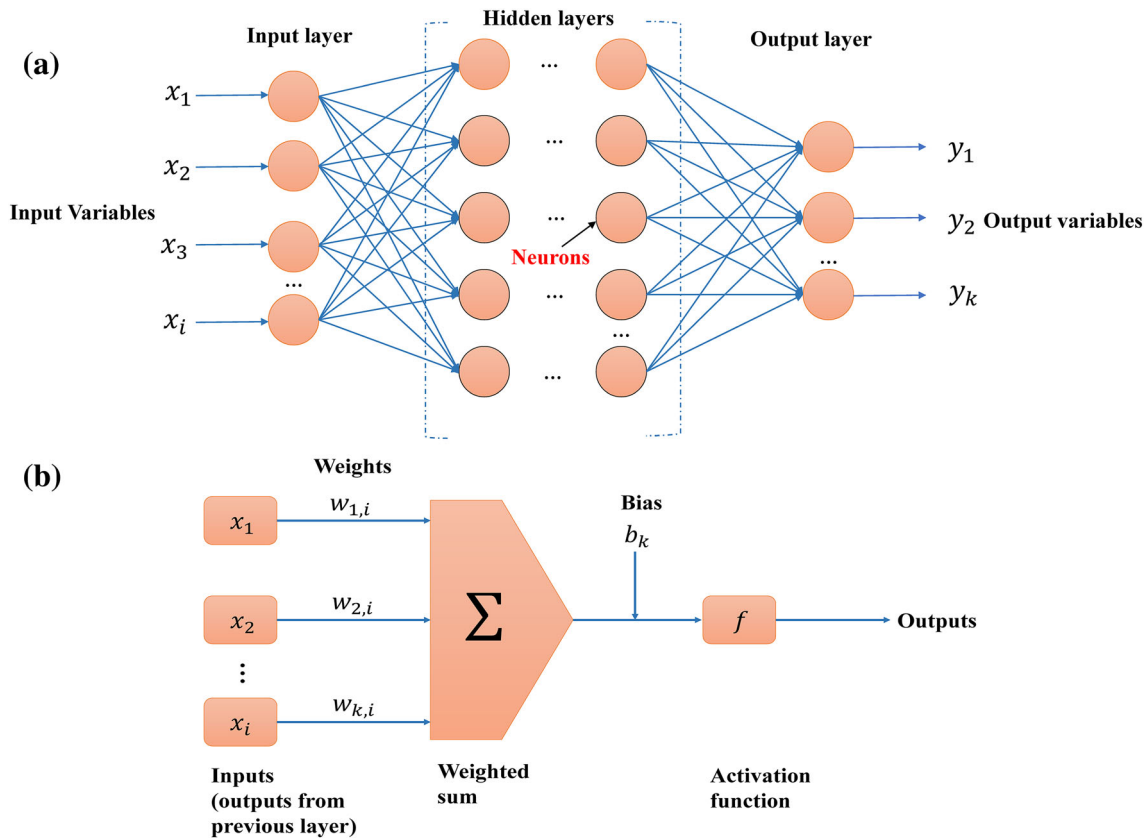


**Figure 1** Topology of backpropagation neural network model. **a** A schematic of a three-layer neural network; **b** schematic of each neuron in the network.

Shi et al. [27] collected a total of 163 alloy 600 CGR data under PWSCC by searching and consulting literature from various channels. All the data collected are derived from the constant load SCC experiments. The training data of various experimental data recorded in the literature are highly dispersed, and the information reflected is inconsistent. Generally, the data in the literature contain the following five basic variables:  $T$  (temperature),  $K_I$  (SIF), degree of cold working and the content of B and Li in solution. In order to unify the experimental data from different experiments, three other variables that have an important influence on PWSCC are determined based on the known five variables: corrosion potential, PH and conductivity of the solution. Table 1 shows the main input parameters for training ANN model and the importance of each input parameter on CGR based on fuzzy curves analysis. The fuzzy curves method is a method proposed by Lin and Cunningham [36] to establish the relationship between input variables and output variables by using fuzzy logic. In other words, the importance of different input

**Table 1** Inputs selected for the artificial neural network [27]

Inputs	Range	Importance
Temperature	290–360 °C	1.7983
$K_I$	4.6–101 MPa $\sqrt{m}$	1.4733
PH	5.52–9.19	1.4026
Conductivity	1.7–1116 $\mu S/cm$	1.3683
ECP	– 1.096 $V_{she}$ to – 0.61 $V_{she}$	1.362
Yield strength	211–500 MPa	1.1577
$B(OH)_3$	0–1800 ppm	0.7379
LiOH	0–10 ppm	0.386

parameters can be determined by the range of their respective fuzzy curves.

Before training the neural network, it is necessary to normalize the input data in order to prevent an input parameter with larger values from becoming the dominant parameter. Meanwhile, since the sigmoid function is usually used as the activation function in the neural network, Eq. (7) is adopted to normalize the input variable to the range of 0–1:

$$\hat{x}_i^{(m)} = \frac{\hat{x}_i^{(m)} - \min_{n=1,N}(\hat{x}_i^{(n)})}{\max_{n=1,N}(\hat{x}_i^{(n)}) - \min_{n=1,N}(\hat{x}_i^{(n)})} \quad (7)$$

where  $x_i$  is the original data and  $\hat{x}_i$  is the normalized data. The preprocessed data will be randomly divided into three categories: training data and validation data for training neural networks, and test data for testing neural networks after network training.

When the weights and deviations of the neural network are initialized, the Levenberg–Marquardt backpropagation (LMBP) algorithm [37] can be used for training [26, 27, 35, 38]. The training process is carried out in a circular manner. In each cycle, the neural network's response to the training data is evaluated by the mean variance formula, as shown in Eq. (8). According to the evaluation result, the weight will be updated in the next cycle, and the updated weight will reduce the mean variance, and this process will be repeated until the minimum variance is reached or a termination condition is met:

$$\text{mes} = \frac{1}{N} \sum_{i=1}^N (e_i)^2 = \frac{1}{N} \sum_{i=1}^N (t_i - y_i)^2 \quad (8)$$

where mes is the mean variance,  $N$  is the total number of samples,  $y_i$  is the prediction result of the neural network and  $t_i$  is the target result.

Temperature is an important factor affecting CGR of alloy 600 in PWSCC in dilute solution. Figure 2 shows the relationship between CGR and

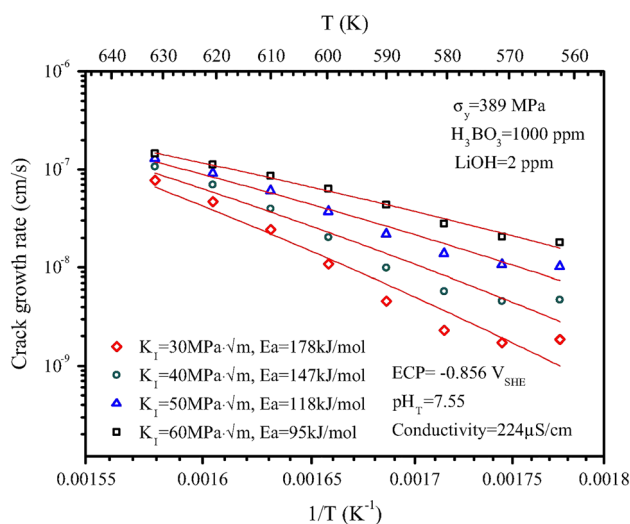


**Figure 2** Effect of temperature on crack growth rate in alloy 600 in PWR primary coolant as a function of stress intensity factor [27].

temperature under different stress intensity factors predicted by ANNs model. The result shows that the activation energy of CGR decreases with the increase in SIF. At higher stress intensities, the strain and strain region at the crack tip increase, and the vacancy gap is independent of temperature, which makes nucleation of the vacancy easier. However, at lower stress intensities, the plastic deformation and deformation region at the crack tip will become smaller, which makes it difficult to nucleate the vacancies.

As a purely mathematical empirical model, ANNs are often criticized for their “black box” characteristics, because they do not reveal the intrinsic mechanism of the research system [39]. However, if the structure design of the ANNs is reasonable and the input and output variables are strictly screened, the well-trained and fitted ANNs can still provide help for the elaboration of the intrinsic mechanism of the research object [40]. Additionally, the fuzzy curve analysis has been employed widely and has proven to be effective in identifying the contributions of the independent variables to the dependent variables [29, 41]. Generally speaking, there is still some incompleteness in exploring the mechanism of SCC by ANNs model at present, but ANNs provide a solution to complex SCC systems that are difficult to predict with mathematical models. They can make accurate predictions by learning existing data. Another advantage of ANNs is that the range of prediction can exceed the range covered by experimental data, and the prediction results can enable people to study a complex SCC problem more deeply.

### Deterministic prediction model based on SCC mechanism

It has been shown that the SCC process of austenitic stainless steel and nickel-based alloy in high-temperature water environment of nuclear reactor is a slow and stable crack propagation process caused by three factors: corrosion medium at crack tip, material properties and mechanical state. Due to the complexity of this process and the importance of quantitatively predicting SCC growth rates, many scholars have proposed different mechanisms or models to explain the phenomenon of SCC scientifically. Some of these mechanisms or models are quantitative

formulas, and others are qualitative explanations. No mechanism or model has been proved to be able to explain or predict the effect of all influencing factors on SCC. The following section mainly introduces some of more important mechanisms and corresponding models.

### Slip-oxidation model

The slip-oxidation model is a commonly accepted and adopted model developed by Peter Ford and Peter Andresen [42, 43], also known as the film rupture slip dissolution model or Ford–Andresen model. The term slip-oxidation model in SCC is generally understood as the oldest and simplest film rupture mechanism [44], and the mechanism of SCC is shown in Fig. 3 [45]. Scully [46], Vermilyea [47] and Parkins [48, 49] have done a lot of theoretical and experimental works on the oxide film rupture mechanism of SCC. The oxide film formed on the bare metal surface ruptures under the action of strain, and the matrix metal dissolves to make the crack advance. Subsequently, the oxide film at the crack tip is gradually reformed, resulting in repassivation and crack propagation stops. However, under the action of the crack tip strain, the oxide film ruptures again and the above process is repeated. The crack propagates by way of advancing, stopping and readvancing, leaving a crack arrest line on the fracture, but the crack continues to propagate forward under the combined action of stress and environment, which is the initial film rupture mechanism. Ford believes that it is more accurate to call it “slip oxidation” because crack growth is the result of the combined oxidation reaction of  $M/M^+$  and  $M/MO$  [50]. Ford and Andresen have carried out a large number of experimental studies and concluded that most SCC of metals or alloys in high-temperature water environments can be explained by slip-oxidation mechanism of anodic dissolution [51–54].

Quantitative prediction of CGR by slip-oxidation model is based on Faraday’s law between the oxidation charge density  $Q$  on the surface and the transformation of metallic state to oxide state (e.g.,  $MO$  or  $M_{aq}^+$ ) [50]. Therefore, for a specific material and crack tip environment, the CGR is primarily determined by the change of transient oxidation current density with time and the film rupture rate under the strain state at the crack tip.

According to Faraday’s law, the CGR of the slip-oxidation model can be expressed as.

$$\frac{da}{dt} = \left(\frac{M}{\rho zF}\right) \cdot \left(\frac{Q_d}{t_d}\right) \tag{9}$$

where  $M$  is the atomic mass of the dissolved metal,  $\rho$  is the metal density,  $F$  is the Faraday constant (96500 C/mol),  $z$  is the number of electrons lost in the oxidation reaction,  $t_d$  is the period of mechanical rupture of the oxide film and  $Q_d$  is oxidation charge density within a film rupture cycle  $t_d$ .

The transient oxidation current density at the crack tip changes with time during the slip-oxidation model as shown in Fig. 4. When the crack tip is a completely bare metal, the crack tip has the highest oxidation current density  $i_0$ , but this process has a shorter time  $t_0$ ; then, the crack tip is affected by the surface passivation film (or deposit) and the oxidation current density begins to decay exponentially and reaches a steady passive state at  $t_p$ , where the current density is  $i_p$ :

$$i(t) = i_0 \cdot \left(\frac{t}{t_0}\right)^{-m} \tag{10}$$

$$Q_d = \int_0^{t_d} i(t)dt \tag{11}$$

$$Q_d = Q_I + Q_{II} + Q_{III} \tag{12}$$

$$Q_I = i_0 \cdot t_0 \tag{13}$$

$$Q_{II} = \int_{t_0}^{t_p} i(t)dt \tag{14}$$

$$Q_{III} = i_p \cdot (t_d - t_p) \tag{15}$$

where  $i_0$  and  $t_0$  are constants related to the oxidation of fresh metal surfaces in the environment,  $i(t)$  is the relationship of oxidation current density with time,  $m$  is the oxidation rate decay curve,  $Q_I$  is the oxidation charge during fast steady oxidation,  $Q_{II}$  is the oxidation charge during the recovery period of the protective oxide film,  $Q_{III}$  is the oxidation charge in the steady passive state,  $t_p$  is the time to reach the steady passive state and  $i_p$  is the current density reaching the steady passive state.

It can be seen from the above-mentioned film rupture mechanism that SCC is the result of competition between the film rupture rate and the repassivation rate, and the stress corrosion sensitivity is related to the crack tip strain rate. In addition, assuming that the crack tip strain rate is the oxide

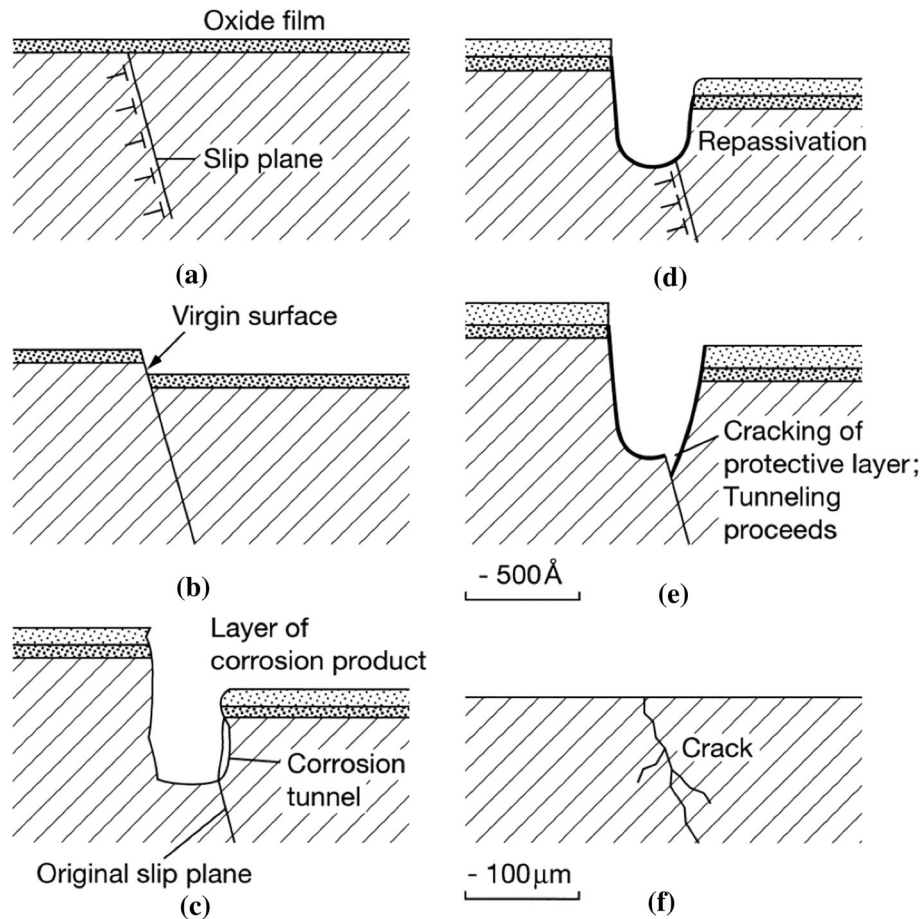


**Figure 3** Schematic diagram of film rupture mechanism for SCC [45]. **a** The metal or alloy forms a layer of oxide film in the corrosive medium, and stress causes dislocations (represented by the  $\perp$  symbol) on the slip surface to start. **b** The dislocation slips out of the surface to create a slipping step, which ruptures the film and exposes the virgin surface. **c** The virgin surface is the anode relative to the passivation film site, which will dissolve locally, and corrosion products will appear in the outer layer. **d** The surface of

the dissolved notch will be repassivated in the solution, and the dissolution will stop after the passivation film is formed again. **e** There is stress concentration at the top of the dissolved area (such as the crack tip or the bottom of the pit), so the repassivation film at this point will rupture through dislocation motion and local dissolution will occur. **f** This cyclical rupture of the film, metal dissolution and repassivation process lead to initiation and propagation of the SCC.

film rupture strain rate, therefore, the oxide film rupture period  $t_d$  can be expressed as

$$t_d = \varepsilon_d / \dot{\varepsilon}_{ct} \quad (16)$$

where  $\varepsilon_d$  is the threshold strain for the rupture of the oxide film and  $\dot{\varepsilon}_{ct}$  is the crack tip strain rate, which can be written as  $d\varepsilon_{ct}/dt$ .

When the metal at the crack tip is exposed ( $\varepsilon_d / \dot{\varepsilon}_{ct} < t_0$ ), the maximum CGR corresponds to

$$\frac{da}{dt_{\max}} = \left( \frac{M}{\rho z F} \right) \cdot i_0 \quad (17)$$

However, under the LWR nuclear power plant environment, nuclear power structural materials are

generally in a constant load or displacement state, in which case the period of film rupture ( $\varepsilon_d / \dot{\varepsilon}_{ct} \gg t_0$ ). At this time, the metal at the crack tip will no longer be exposed. The second stage in Fig. 4 is the main process of stress corrosion crack growth [55], so it can be considered that

$$Q_d = Q_{II} \quad (18)$$

For slip-oxidation model, the CGR prediction formula has been proposed by Ford–Andresen, which is the combination of Eqs. (9–12), (14), (16) and (18):



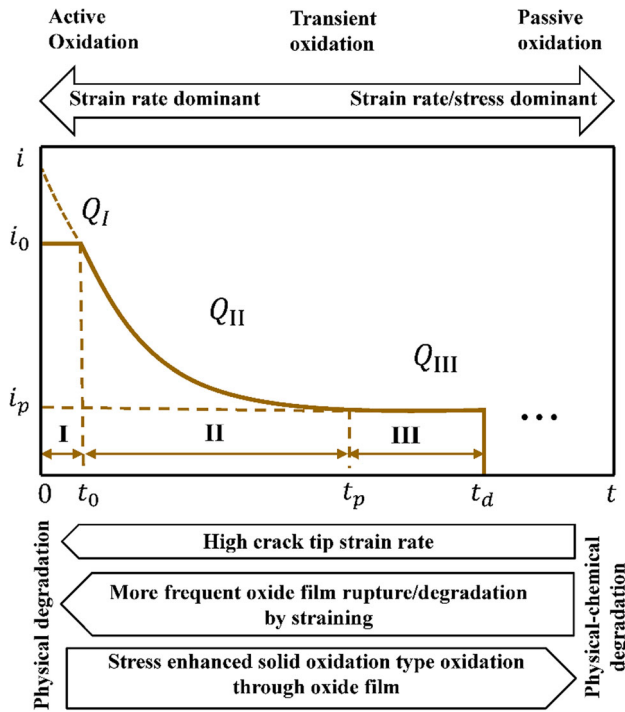


**Figure 4** Schematic diagram of transient oxidation current density at crack tip [55].

$$\frac{da}{dt} = \left( \frac{M}{z \cdot \rho \cdot F} \right) \left( \frac{i_0}{1 - m} \right) \left( \frac{t_0}{\varepsilon_d} \right)^m (\dot{\varepsilon}_{ct})^m \quad (19)$$

It can also be expressed as

$$\frac{da}{dt} = k_a (\dot{\varepsilon}_{ct})^m \quad (20)$$

$$k_a = \left( \frac{M}{z \cdot \rho \cdot F} \right) \left( \frac{i_0}{1 - m} \right) \left( \frac{t_0}{\varepsilon_d} \right) \quad (21)$$

where  $k_a$  is the oxidation rate constant, which is determined by the electrochemical environment and material properties near the crack tip.  $m$  is the passivation rate parameter that is controlled by the crack tip environment (such as pH, corrosion potential, anion concentration) and the material (such as degree of grain-boundary sensitization). In order to have a quantitative description of  $m$ , it is considered as a function of testable system variables, such as the measurable value of bulk coolant conductivity ( $k$ ), corrosion potential at the crack tip ( $\varphi_c$ ) and the degree of grain-boundary sensitization as quantified by electrochemical potentiokinetic reactivation (EPR) parameter [50]:

$$m = \left[ \frac{e^{f(k)}}{e^{f(k)} + e^{g(\varphi_c)}} \right]^{h(\text{EPR})} \quad (22)$$

where  $f, g, g'$  are functional constants.

The slip-oxidation model has obtained a prominent position in the nuclear reactor industry and has been successfully applied to the SCC life prediction of structural materials in nuclear power plants with appropriate on-site practical testing technology. However, the model has also been criticized by some scholars in the application process. Macdonald [56] believes that the model advanced by Ford and Andresen does not conform to charge conservation law. Rebak and Szklarska-Smialowska [6], on the other hand, point out that the slip-oxidation model appears to be simplistic and does not explicitly address variables such as temperature, PH, presence of carbides at the grain boundaries and CW. Gutman [57] considers that the mechanochemical effect was neglected in the process of dissolution acceleration. Hall [58] shows that there are conceptual and mathematical problems with the model development. However, as the most commonly accepted model and a mechanism-based model interpretation, the slip-oxidation model plays a pioneering role in the calculation of CGR. Although the slip-oxidation model cannot fully explain the SCC problem, the CGR model based on the slip-oxidation mechanism is better applied in the service safety design of nuclear power materials. In the future, with the diversification of analytical methods and the further explanation of SCC, slip-oxidation model will be more perfect and play a greater role.

### Crack tip strain rate model

The crack tip strain rate plays an important role in determining the SCC growth rate because it controls the rupture rate of passivation film at the crack tip. Therefore, it is especially important to find a method to accurately predict the crack tip strain rate when establishing a deterministic model of SCC prediction. Many attempts have been made to quantify the crack tip strain rate using numerical and analytical methods. Ford [59] proposed a semiempirical formulation of crack tip strain rate, which was not based on the plastic deformation theory of the crack tip or other fracture mechanisms. The crack tip strain rate is given by

$$\dot{\varepsilon}_{ct} = 4.1 \times 10^{-14} \text{K}^{-4} \quad (23)$$

The calculated results of CGR by Eq. (23) are in good agreement with the observed values. However, an important disadvantage of this formula is that it cannot perfectly reflect the effect of stress intensity on CGR.

Congleton et al. [60] expression for the crack tip strain rate is based on linear elastic fracture mechanics and hence has a good theoretical basis [61, 62], especially for brittle solids:

$$\dot{\epsilon}_{ct} = \frac{\dot{a}}{r} \left[ 63.653\pi\alpha \frac{(1-\nu^2)}{\sigma_y E} + \beta \left( \frac{\sigma_y}{E} \right) \ln \left( \frac{R}{r} \right) \right] \quad (24)$$

where  $r$  is the distance of the opening displacement from the crack tip,  $\nu$  is the Poisson's ratio,  $\sigma_y$  is the yield strength,  $E$  is the elastic modulus,  $\alpha$  and  $\beta$  are the material constants, and  $R$  is the scale factor of the plastic zone at the crack tip.

However, Eq. (24) cannot be applied to work-hardening materials and the critical SIF cannot be predicted.

Shoji et al. from the Fracture Research Institute (FRI) proposed a crack tip strain rate model [55, 63, 64] based on the theory of crack tip strain gradient and strain redistribution theory of the extended crack front, which is also known as FRI model or Shoji model in the field of international EAC research. Figure 5 is a schematic diagram of the electrochemical environment, material and mechanical state at the crack tip of nuclear power structure materials in a high-temperature water environment.

Hutchinson–Rice–Rosengren (HRR) field [65, 66], Gao–Hwang (GH) field [67] and Gao–Zhang–Hwang (GZH) field [68] can well fit the crack tip strain

distribution of strain-hardening materials according to different descriptions of asymptotic field at the crack tip [69–71]. In this paper, Gao–Hwang's description of the asymptotic field at the crack tip is used to calculate the plastic strain rate at the crack tip.

For strain-hardening materials, the stress–strain curve is expressed by Gao–Hwang's definition as follows:

$$\epsilon = \begin{cases} \frac{\sigma}{E} & \text{for } \sigma \leq \sigma_0 \\ \frac{\sigma}{E} + C(\sigma - \sigma_0)^{n_{GH}} & \text{for } \sigma > \sigma_0 \end{cases} \quad (25)$$

where  $\sigma$  and  $\epsilon$  are the true stress and the true strain, respectively,  $\sigma_0$  is the initial yield strength,  $C$  is the offset coefficient and  $n_{GH}$  is the strain-hardening exponent in the stress–strain relationship of Gao–Hwang.

Gao–Hwang takes into account the plastic strain in the whole range, so it is often used to describe the crack tip asymptotic field of nuclear structural materials with strong strain-hardening ability. Under the condition of plane strain, the plastic strain  $\epsilon_p$  can be expressed as

$$\epsilon_p = \beta \left( \frac{\sigma_y}{E} \right) \left[ \ln \left( \frac{R_p}{r} \right) \right]^{\frac{n_{GH}}{n_{GH}-1}} \quad (26)$$

The plastic zone size  $R_p$  is

$$R_p = \lambda \left( \frac{K}{\sigma_y} \right)^2 \quad (27)$$

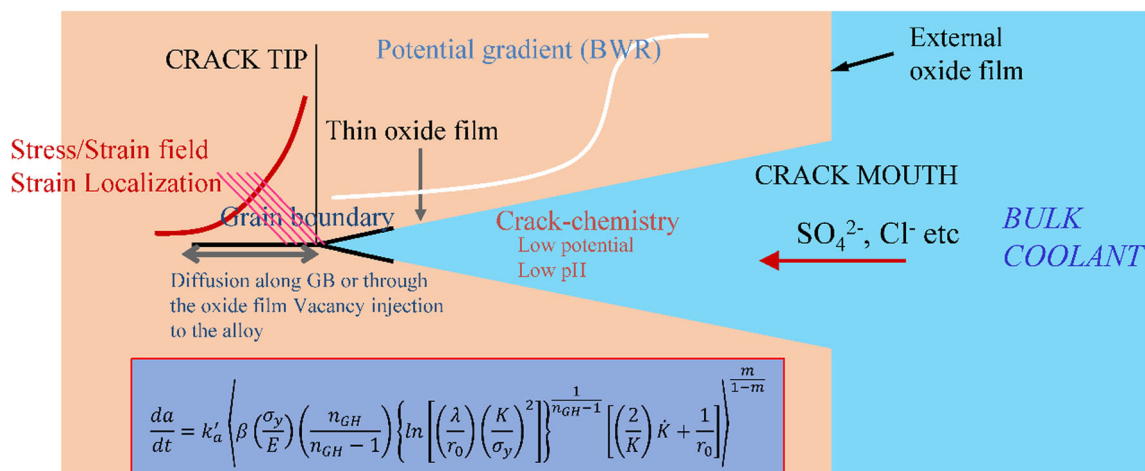


**Figure 5** Schematic of electrochemical environment, material and mechanical state at the crack tip of nuclear power structural materials in high-temperature water environment.

where  $r$  is the distance from a growing crack tip and  $\lambda$  is the constraint factor and a dimensionless constant.

The plastic strain  $\varepsilon_p$  is proposed to substitute the plastic strain  $\varepsilon_{ct}$  at a characteristic distance  $r_0$  in front of the crack tip:

$$\varepsilon_{ct} = \varepsilon_p|_{r=r_0} \tag{28}$$

Shoji et al. [63] put forward a crack tip strain rate model based on the theory of strain gradient at the crack tip and strain redistribution as the crack advances, Eqs. (29) and (30). In the case where the stress intensity factor  $K$  is constant, the first term of formula (30) is negligible:

$$\frac{d\varepsilon_{ct}}{dt} = \left(\frac{d\varepsilon_{ct}}{da}\right) \cdot \left(\frac{da}{dt}\right) \tag{29}$$

$$\left(\frac{d\varepsilon_{ct}}{da}\right) = \frac{\partial \varepsilon_{ct}}{\partial a} - \frac{\partial \varepsilon_{ct}}{\partial r} \tag{30}$$

Combining the theory of crack tip strain gradient with the theory of Gao–Hwang crack tip asymptotic field, i.e., Eqs. (26–30), the crack tip strain rate model can be expressed as

$$\begin{aligned} \frac{d\varepsilon_{ct}}{dt} = & \beta \left(\frac{\sigma_y}{E}\right) \left(\frac{n_{GH}}{n_{GH}-1}\right) \left\{ \ln \left[ \frac{\lambda}{r_0} \left(\frac{K}{\sigma_y}\right)^2 \right] \right\}^{\frac{1}{n_{GH}-1}} \\ & \times \left[ \left(\frac{2}{K}\right) \dot{K} + \left(\frac{1}{r_0}\right) \left(\frac{da}{dt}\right) \right] \end{aligned} \tag{31}$$

where  $\dot{K}$  (or  $dK/dt$ ) is the change rate of stress intensity factor. When the crack grows under constant load conditions, that is, when  $\dot{K} = 0$ , the formula is

$$\begin{aligned} \frac{d\varepsilon_{ct}}{dt} = & \beta \left(\frac{\sigma_y}{E}\right) \left(\frac{n_{GH}}{n_{GH}-1}\right) \left\{ \ln \left[ \frac{\lambda}{r_0} \left(\frac{K}{\sigma_y}\right)^2 \right] \right\}^{\frac{1}{n_{GH}-1}} \\ & \times \left[ \left(\frac{1}{r_0}\right) \left(\frac{da}{dt}\right) \right] \end{aligned} \tag{32}$$

The CGR growth rate can be calculated by substituting Eqs. (32) into (19):

$$\begin{aligned} \frac{da}{dt} = & k'_a \left\langle \beta \left(\frac{\sigma_y}{E}\right) \left(\frac{n_{GH}}{n_{GH}-1}\right) \left\{ \ln \left[ \frac{\lambda}{r_0} \left(\frac{K}{\sigma_y}\right)^2 \right] \right\}^{\frac{1}{n_{GH}-1}} \right. \\ & \left. \times \left[ \left(\frac{2}{K}\right) \dot{K} + \left(\frac{1}{r_0}\right) \left(\frac{da}{dt}\right) \right] \right\rangle^{\frac{m}{1-m}} \end{aligned} \tag{33}$$

where

$$k'_a = (k_a)^{\frac{1}{1-m}} = \left[ \left(\frac{M}{z \cdot \rho \cdot F}\right) \left(\frac{i_0}{1-m}\right) \left(\frac{t_0}{\varepsilon_d}\right) \right]^{\frac{1}{1-m}} \tag{34}$$

Based on the theory of slip dissolution/oxidation, the model is calculated by Faraday’s law of electrochemistry and strain–stress field of strain-hardening material. The electrochemical environment, material and mechanical factors of crack tip are organically combined in formula (33), which can quantitatively predict the SCC growth rate of nuclear power structural materials in high-temperature water environment and analyze the influence of crack tip corrosion environment, material and mechanical parameters on CGR. At present, it has become the basic theoretical model in the field of EAC research of nuclear power structural materials in Japan’s high-temperature water environment and has also been adopted by many relevant laboratories and researchers in the world [72].

However, the obtained formula of crack tip strain rate model is very complex, so it is difficult to analyze and calculate. Moreover, the formula contains a large number of parameters, and the physical meaning represented by the combination is not clear enough, and the quantized precision is difficult to guarantee. Therefore, it is far from the actual engineering application.

### Coupled environment fracture model

The coupled environment fracture model (CEFM) was proposed by Macdonald et al. [73], which was originally used to predict the SCC growth rate of sensitized 304 stainless steel in the LWR environment. Crack advance is assumed to occur via the slip-oxidation/dissolution mechanism, but the model emphasized that the coupling between internal and external environment and charge conservation are the key factors to determine the CGR [56]. Macdonald et al. continued to improve the model, calculated the potential distribution inside and outside the crack according to the Laplace equation and the Butler–Volmer equation and gradually calculated the CGR using a more accurate crack tip strain rate model, and then the influence of temperature on the strain rate at the crack tip is taken into account by the Arrhenius formula, which allows the CEFM model to predict the stress corrosion damage at the start and end of the boiling water reactor (BWR) because the electrochemical properties of the coolant change with

temperature during these two phases, and the effect of sulfuric acid on the crack growth rate is also considered in the model [74, 75]. At present, the scope of application of this model has gradually broadened, its applicable system extends from high-temperature high-pressure water environment to room-temperature solution [76], the material extends from stainless steel to carbon steel [77, 78], aluminum–magnesium alloy [76] and nickel-based alloy [79], the corrosion type extends from SCC to corrosion fatigue [80], pitting corrosion [81], crevice corrosion [82, 83] and hydrogen-induced cracking (HIC) [10] and the predicted form also extends from initial CGR to crack shape evolution [84].

The physico-electrochemical basis of the CEFM is the differential aeration hypothesis (DAH). According to the theoretical assumption, the local corrosion is caused by the spatial separation of the local anode and the local cathode, as shown in Fig. 6. Local anode exists inside the crack, while local cathode exists on the exposed surface. The positive current flows from the inside of the crack to the outer surface of the crack through the solution, and the negative current flows from the crack to the outer surface of the crack

through the metal. The two currents are neutralized by the charge transfer reaction on the outer surface of the crack, which is also referred to as the coupling current. One of the main characteristics of the CFEM model based on DAH is that the sum of the reaction currents inside and outside the crack is zero. The corresponding expressions are as follows:

$$i_{\text{crack}} A_{\text{crack-mouth}} + \int_s i_c^N ds = 0 \quad (35)$$

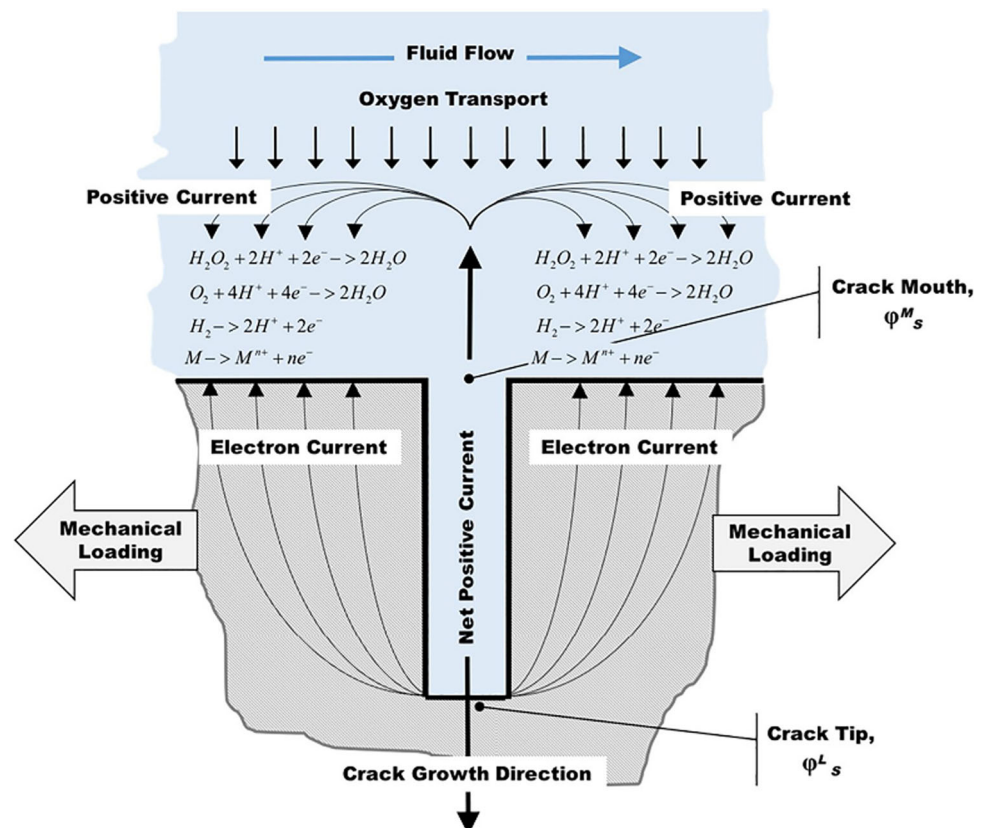
or equivalently

$$\int_s i^N ds' = 0 \quad (36)$$

where  $i_{\text{crack}}$  is the net (positive) current density flowing from the crack mouth,  $A_{\text{crack-mouth}}$  is the crack mouth area,  $i_c^N$  is the net (cathode) current density due to charge transfer reaction on the external surface,  $i^N$  is the net current density,  $ds$  and  $ds'$  are the area increments of the outer surface and the entire area, respectively, and the subscript “ $s$ ” on the integral indicates integration over the entire outer surface.

The calculation of SCC growth rate by CEFM is divided into two steps. Firstly, the electrochemical

**Figure 6** Coupling of crack internal and external environments [79].



corrosion potential (ECP or  $E_{\text{corr}}$ ) at the outer surface of the crack is calculated, and then the crack growth rate is estimated.

It is assumed that the potential  $\varphi_s^\infty$  relatively far from the crack position does not change with the existence of the crack, because the value is equal to ECP and the potential sign is opposite. The ECP is calculated by the mixed potential model (MPM) [85], which considers that the hydrogen electrode reaction (HER) ( $\text{H}_2 + 2\text{OH}^- \leftrightarrow \text{H}_2\text{O} + 2\text{e}^-$ ), the oxygen electrode reaction (OER) ( $4\text{OH}^- \leftrightarrow \text{O}_2 + 2\text{H}_2\text{O} + 4\text{e}^-$ ), the hydrogen peroxide electrode reaction (HPER) ( $2\text{OH}^- \leftrightarrow \text{H}_2\text{O}_2 + 2\text{e}^-$ ) and dissolution of the outer surface oxide film depend on the environmental composition [79]. Therefore, the net (cathode) current of the surface is given by the following formula:

$$i_c^N = i(\text{H}_2) + i(\text{O}_2) + i(\text{H}_2\text{O}_2) + i_{\text{diss}} \quad (37)$$

where  $i(\text{H}_2)$ ,  $i(\text{O}_2)$  and  $i(\text{H}_2\text{O}_2)$  are partial current densities of the HER, OER and HPER, respectively, with the sign of the current depending on the sign of the ECP relative to the equilibrium potential  $E_e$  O/R, and  $j$  is the reaction index [ $j = 1$  for the HER,  $j = 2$  for the OER, and  $j = 3$  for the HPER], and  $i_{\text{diss}}$  is the dissolved current density of metal alloy oxide film. The current density for the oxidation or reduction of the electroactive substance X on the outer surface is expressed by the generalized Butler–Volmer equation (GBVE):

$$i_{\text{O/R},j} = \frac{e^{\eta_j/b_{a,j}} - e^{\eta_j/b_{c,j}}}{\frac{1}{i_{\text{O/R},j}^0} + \frac{e^{\eta_j/b_{a,j}}}{i_{l,f,j}} - \frac{e^{-\eta_j/b_{a,j}}}{i_{l,r,j}}} \quad (38)$$

where  $\eta_j = E - E_{\text{O/R},j}^e$  is the overpotential for reaction  $j$ ,  $i_{\text{O/R},j}^0$  is the exchange current density of reaction  $j$ ,  $i_{l,f,j}$  is the mass transfer limit current density of forward oxidation reaction,  $i_{l,r,j}$  is the corresponding quantity of the reverse reduction reaction and the parameters  $b_{a,j}$  and  $b_{c,j}$  are the forward and reverse Tafel constants.

In order to solve the current emanating from the crack mouth, it is necessary to calculate the potential distribution at the interface according to the distance between the crack mouth and the outer surface. This is achieved by solving Laplace’s equation [74]:

$$\nabla^2 \varphi_s = 0 \quad (39)$$

Obtain  $\varphi_{s(x)}$  so that the electrical neutrality outside the crack is satisfied at all points. When  $\varphi_{s(x)}$  is known, the potential  $\varphi_{s(0)}$  at the crack opening can be calculated and the potential distribution equation under the crack can be solved.

The electrochemical dissolution reaction occurring at the crack tip from oxidation of the alloy is described in terms of Tafel equation, so as to obtain the average current in the slip-oxidation/dissolution/repassivation cycle:

$$I_0 = 2i_{\text{O}}^0 A_{\text{ct}} \left( \frac{t_0}{t_f} \right) e^{\frac{\varphi_s^L - \varphi_s^0}{b_a}} \quad (40)$$

where  $i_{\text{O}}^0$  is the standard exchange current density,  $A_{\text{ct}}$  is the average area of the activated crack tip,  $\varphi_s^L$  is the potential in the solution near the crack tip,  $\varphi_s^0$  is the crack tip (negative) standard potential  $\varphi_M^0$ ,  $b_a$  is Tafel constant,  $I_0$  is the total current of the crack exit,  $t_f$  is the crack cycle time of the crack tip passivation film and  $t_0$  is the constant determined by the repassivation transient.

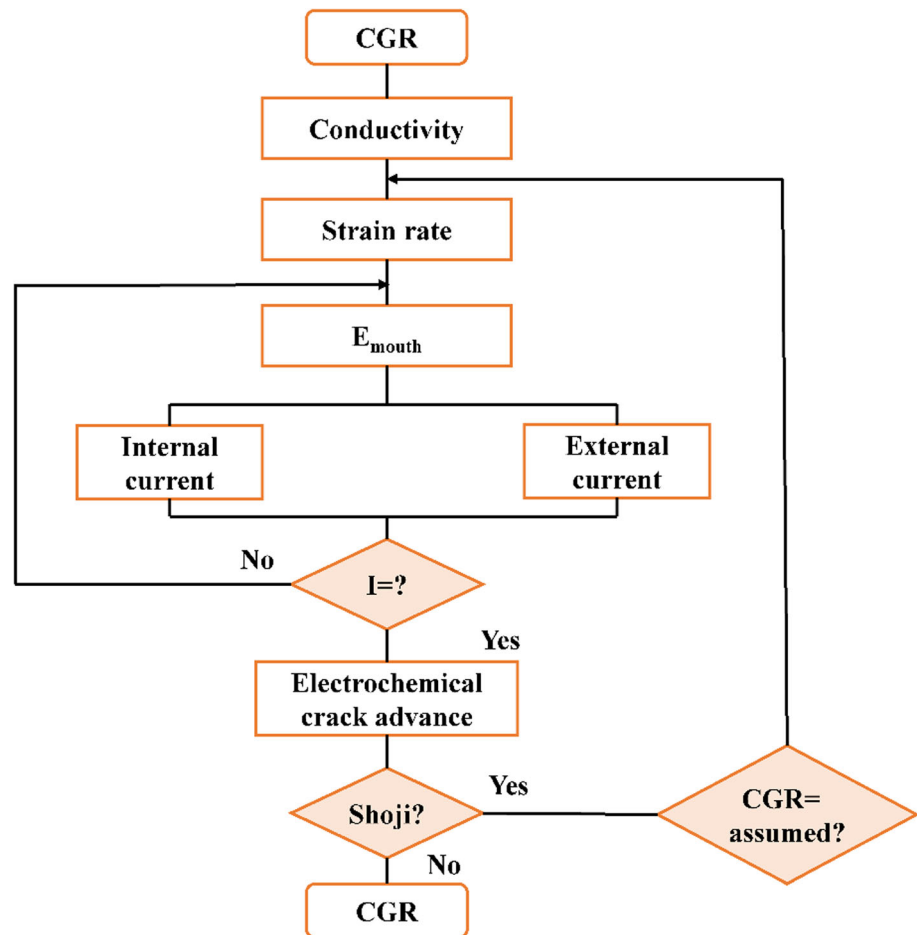
Once  $\varphi_s^0$  and  $\varphi_M^0$  are known, the potential distribution along the crack (passing distance  $x$ ) in the crack environment can be estimated by solving the Laplace equation. However, since  $\varphi_s^0$  and  $\varphi_s^L$  depend on  $I_0$ , the above calculation must be repeated until the convergence of the total current is obtained [74]. The CGR is calculated using Faraday’s law:

$$\frac{dL}{dt} = \frac{MI_0}{z\rho FA_{\text{ct}}} \quad (41)$$

CEFM model is widely used in various corrosion damage prediction programs developed by Macdonald (such as DAMAGE-PREDICTOR, ALERT, REMAIN, FOCUS, etc.) to predict the SCC failure of the main cooling circuit in boiling water reactor environment. So far, the DAMAGE-PREDICTOR program has simulated 14 boiling water reactor nuclear power plants worldwide, and the field test data fully verify the accuracy of the prediction data of the model. Figure 7 shows the flow of CEFM model calculation. The program based on CFEM model can effectively predict the SCC growth rate.

There is also some controversy about the CEFM in academia. For example, Andresen and Ford, who proposed the slip-oxidation model, argued that CEFM could not explain the different effects of different impurity anions on SCC under the same conductivity [86]. Macdonald believed that the effects of

**Figure 7** Flowchart of the CEFM for calculating CGRs.



different ions could be reflected in the process of conductivity calculation and charge transfer reaction from the model [87]. Andresen and Ford also argued that it was not safe to rely solely on the potential gradient for particle transport inside the crack in the CEFM model, but this opinion was also denied by Macdonald. Rebak and Szklarska-Smialowska believed that CEFM could not predict the cracking of alloy 600 under open circuit potential and external cathodic potential in high-temperature water [6]. The most significant difference between the CEFM model and other SCC growth rate models is that the model considers that the positive current is consumed at the outer surface of the crack by the reduction reaction of the cathode depolarizer (such as oxygen reduction reaction or hydrogen evolution reaction), which also means strong electrochemical coupling between the inside and the outside. The outer surface of the material is a part of any local corrosion deterministic model that cannot be ignored. However, the CEFM

model is the only deterministic model that considers this factor.

### Surface mobility mechanism

The SCC surface mobility mechanism (SMM) was first introduced by Galvele in 1986 [88] and was fully formulated in 1987 [89] which was mainly derived from the publications made on surface self-diffusion of metals. This mechanism can predict the specificity of SCC, as well as the effect of temperature on SCC, and the increase in crack velocity by hydrogen. An improved version given in 1993 [90] shows that the role of the environment is not only to change the surface self-diffusivity of the metal or alloy, but also to supply the metal surface with the vacancies consumed by the crack propagation process. The atoms at the crack tip move from the high-stress region to the low-stress region inside the crack by surface diffusion, so that the crack grows an atom-gap distance. Crack propagation occurs when the stressed lattice at

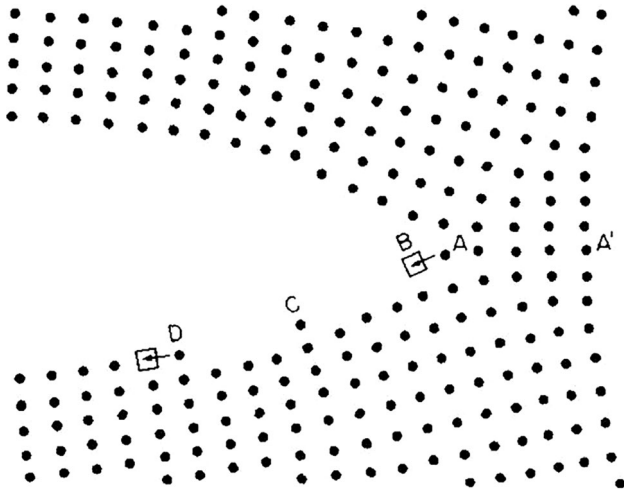


**Figure 8** A schematic description of surface mobility cracking mechanism [89].

the tip of the crack captures the vacancies according to the schematic description of Fig. 8. Surface mobility could be acting in systems where the presence of specific metal cations in the solution is essential. Galvele [91] also concluded that the SCC SMM is a very promising tool for predicting the SCC sensitivity of metals and alloys, especially in the nuclear power industry.

The CGR based on SMM is given by the following equation [92]:

$$\frac{da}{dt} = \frac{D_S}{L} \left[ \exp\left(\frac{\sigma a^3}{kT}\right) - 1 \right] \tag{42}$$

where  $D_S$  is the surface self-diffusion coefficient,  $L$  is the diffusion distance of the vacancies (typically  $10^{-8}$  m),  $a$  is the atomic diameter,  $\sigma$  is the elastic surface stress at the crack tip and  $k$  is the Boltzmann constant.

The value of  $D_S$  is not readily measurable but can be roughly estimated by two Arrhenius factors, each of which depends on the ratio of the melting temperature  $T_m$  to the ambient temperature  $T$ :

$$D_S = 7.4 \times 10^{-2} \exp\left(-\frac{30T_m}{RT}\right) + 1.4 \times 10^{-6} \exp\left(-\frac{13T_m}{RT}\right) \tag{43}$$

To account for the effect of hydrogen on the CGR, the following equation was suggested: [93]

$$\frac{da}{dt} = \frac{D_S}{L} \left[ \exp\left(\frac{\sigma a^3 + \alpha E_b}{kT}\right) - 1 \right] \tag{44}$$

where  $E_b$  is the binding energy of  $H$ -single vacancy, and  $\alpha$  is a dimensionless function, which is used to measure the difference between the hydrogen saturation degree of vacancy in the stress region and that in the no-stress region.

The SCC SMM has succeeded in explaining numerous SCC situations, in which deleterious films are formed on the metal surface. However, Sieradzki and Friedersdor [94] stated that the SMM overestimated the CGR by 14 orders of magnitude for ductile fcc metals. Galvele [95] argued that they erroneously calculated the surface vacancy concentrations with equations developed for metals in the absence of a corrosive environment. Gutman [96] commented that the CGR calculated by SMM is only the creep deformation rate of Nabarro–Herring and can never be numerically equal to the CGR. Galvele [93] concluded that they never used an equation for creep to calculate the CGR. SMM proposes a universal mechanism, which can interpret SCC not only under constant load, but also under constant strain rate test. SMM based on the concept of stress self-diffusion mass transfer plays an important role in the study of SCC, but unfortunately some assumptions are not perfect. Moreover, there are not enough experiments to confirm this problem, but we hope the model can be more perfect. One of the most promising characteristics of SCC SMM is that it allows the prediction of crack velocity at any temperature if the crack velocity at a given temperature is known.

### Prediction model combining calculation and simulation with SCC mechanism

In recent years, material calculation and simulation have been rapidly developed, which have made breakthroughs in the study of corrosion mechanism and has a positive guiding role in the design and use of materials. At present, the most widely used computational methods in the field of corrosion include first-principles and molecular dynamics methods based on density functional theory (DFT), molecular dynamics (MD) calculations based on Newtonian mechanics, thermodynamic and kinetic calculations based on electrochemistry and finite element method (FEM) based on fracture mechanics. Calculation and simulation have become the third way to discover

new concepts and mechanisms after experiments and theories [97].

### FEM based on fracture mechanics

With the rapid development of computer technology, the application of FEM in SCC growth simulation is more and more extensive, which mainly focuses on two aspects: determining a single parameter in the SCC growth rate prediction model based on fracture mechanics and simulation analysis of SCC growth based on slip-oxidation/dissolution theory.

Most SCC growth rate prediction models need to obtain the crack tip strain rate first, and the change rate of SIF is the primary condition for determining the crack tip strain rate. Satoh et al. [98] adopted the finite element crack propagation simulation method of nodal force release technique and slow strain rate tensile test to obtain  $dK/dt$  by calculating the SIF values at different moments and further obtained the crack tip strain rate. The theoretical model and finite element simulation are compared from the angle of film rupture strain. Xue and Shoji [99, 100] solved the tensile plastic strain rate  $d\varepsilon_p/da$  at the characteristic distance  $r_0$  based on the elastic–plastic finite element method (EPFEM) and combined with the crack tip strain rate model to obtain the SCC growth rate. With the deepening of research, Xue et al. studied the mechanism of SCC growth rate of stainless steel or nickel-based alloy in LWR environment with single tensile overload [101], SIF [102], crack tip oxide film [103], mechanical properties [104] and scratches [105] based on EPFEM.

According to Eqs. (20), (28), (29), the SCC growth rate of nuclear power structural materials in LWR environment is obtained:

$$\frac{da}{dt} = (k_a)^{\frac{1}{1-m}} \cdot \left( \frac{d\varepsilon_p}{da} \right)^{\frac{m}{1-m}} \quad (45)$$

It can also be expressed as

$$\frac{da}{dt} = k'_a \left( \frac{d\varepsilon_p}{da} \right)^{\frac{m}{1-m}} \quad (46)$$

where the relationship between  $k_a$  and  $k'_a$  is expressed by Eq. (34). It can be obtained from Eq. (46) that the plastic strain rate of the crack tip is intrinsically consistent with the crack growth rate for the electrochemical environment in which the crack tip of a material is fixed.

The  $\Delta a$  and  $\Delta\varepsilon_p$  of the steady-state extended crack front are shown in Fig. 9a. When the crack length increases from  $a_i$  to  $a_{i+1}$ , the tensile plastic strains  $\varepsilon_{p1}$  and  $\varepsilon_{p2}$  can be calculated by FEM, and the corresponding  $d\varepsilon_p/da$  can be obtained by

$$\frac{d\varepsilon_p}{da} \approx \frac{\Delta\varepsilon_p}{\Delta a} = \frac{\varepsilon_{p2} - \varepsilon_{p1}}{a_{i+1} - a_i} \quad (47)$$

where the crack lengths are  $a_i$  and  $a_{i+1}$ ,  $\varepsilon_{p1}$  and  $\varepsilon_{p2}$  correspond to the tensile plastic strain at  $r_0$ , respectively.

The  $\Delta r$  and  $\Delta\varepsilon_p$  of the static crack front are shown in Fig. 9b. At the characteristic distance  $r_0$  of the crack, when the crack length increases  $\Delta r$ , the tensile plastic strains  $\varepsilon_{p1}$  and  $\varepsilon_{p2}$  can be calculated by finite element method. When  $\Delta r$  is very small, the approximation is

$$\frac{d\varepsilon_p}{da} \approx \frac{d\varepsilon_p}{dr} = \frac{\varepsilon_{p2} - \varepsilon_{p1}}{\Delta r} \quad (48)$$

When the crack length increases  $\Delta r$ , the tensile plastic strain rate  $\dot{\varepsilon}_{ct}$  at the characteristic distance  $r_0$  is easily determined from the tensile plastic strains  $\varepsilon_{p1}$  and  $\varepsilon_{p2}$  at the crack tip.

According to Eq. (45), the strain rate  $\dot{\varepsilon}_{ct}$  at the stress corrosion crack tip is replaced by the strain gradient of the crack front. The physical meaning is clear and the SCC growth rate is easy to obtain, which is convenient for engineering application.

Jivkov proposed a boundary moving method based on FEM to simulate the corrosion phenomenon of materials caused by chemical action and established a strain-driven SCC growth model, in which the selection problem of crack growth criterion and path criterion was not required. In this model, the nucleation and growth of corrosion cracks were studied [106–108]. Each crack growth process was divided into the “rupture–dissolution–passivation” process of the oxide film, and the process of crack growth was continuous. It was found that the initiation and growth of cracks were independent of the initial defect size. The crack growth process is divided into two stages: slow crack growth and stable growth, and the CGR of the stable growth phase is independent of the initial defect size [109]. Based on this, Jivkov et al. [110, 111] attempted to use 2D and 3D FEM to simulate the mechanical model of IGSCC. As shown in Fig. 10a, the grain boundary on the mesoscale is simulated by hexagonal beam elements in the 2D model, and the failure strain of the grain boundary is



**Figure 9** Theoretical basis for quantitatively estimating SCC growth. **a** Relation between  $\Delta a$  and  $\Delta \epsilon_p$  of the growing crack tip; **b** relation between  $\Delta r$  and  $\Delta \epsilon_p$  of the stationary crack tip [99].

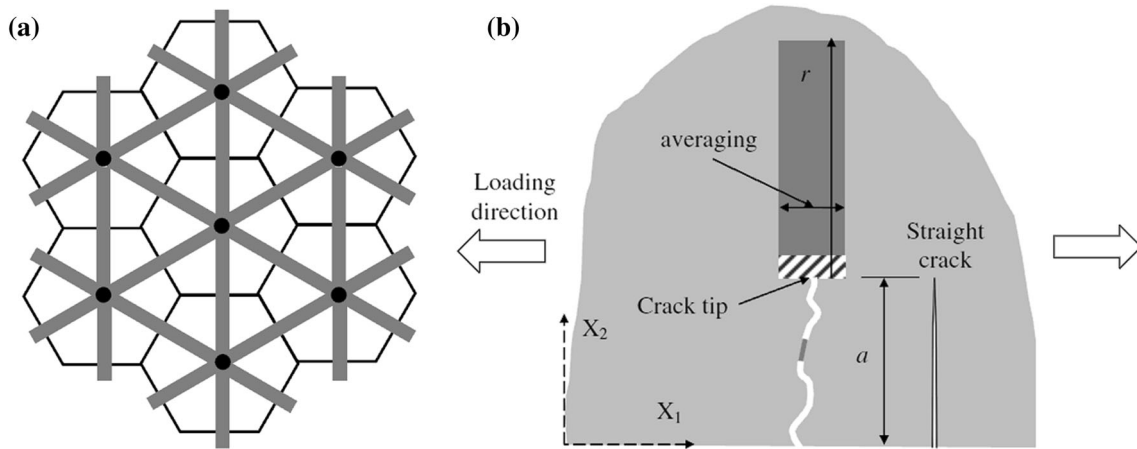
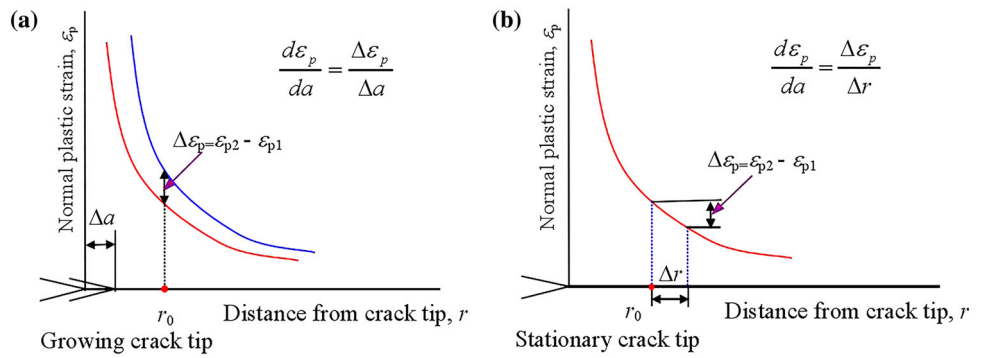


**Figure 10** A two-dimensional mesoscale model for IGSCC growth. **a** Discrete model for the 2D hexagonal structure; **b** SIF calculation for the bridge crack in the finite element model, compared to a straight edge crack [110].

assumed: For the grain boundary which is not resistant to crack growth, the failure strain is considered to be 0.1 times the yield strain, i.e.,  $\epsilon_{sf} = 0.1\epsilon_y$ ; for the grain boundary capable of resisting crack growth, the failure strain is considered to be ten times, i.e.,  $\epsilon_{sf} = 10\epsilon_y$ . According to this hypothesis, the crack growth is predicted, and the calculation method of the SIF is shown in Fig. 10b. The results show that grain boundaries have retarding effect on crack growth, and it is possible to simulate the corrosion process containing chemical action by using the FEM.

The extended finite element method (XFEM) is a numerical method for solving discontinuous mechanics problems proposed by Belytschko and Black in 1999 [112]. It inherits all the advantages of the conventional finite element method (CFEM) and is particularly effective in simulating discontinuities such as interface and crack growth; as a result, XFEM is quickly applied to SCC growth. LEE [113] developed a user subroutine based on the strain rate damage model (SRDM) and applied XFEM to

evaluate the PWSCC growth rate of alloys 600 and 690. Kang and LEE [114, 115] applied the empirical SRDM and XFEM to simulate the initiation and propagation of PWSCC crack and proposed a representative model for PWSCC initiation and propagation based on XFEM.

Although the crack propagation simulation technology based on FEM is a new research method of SCC crack growth, there is little research on the relationship between SCC crack growth and time and it has not been used as an effective means to prevent stress corrosion damage. Therefore, the SCC growth rates simulation based on stress corrosion time correlation is the focus of further research work.

### Multiscale method based on quantum mechanics

SCC is a process of nucleation and propagation of microcracks under the coupling action of corrosion and stress, and the nucleation of microcracks is caused by the breakage of atomic bonds. Therefore,

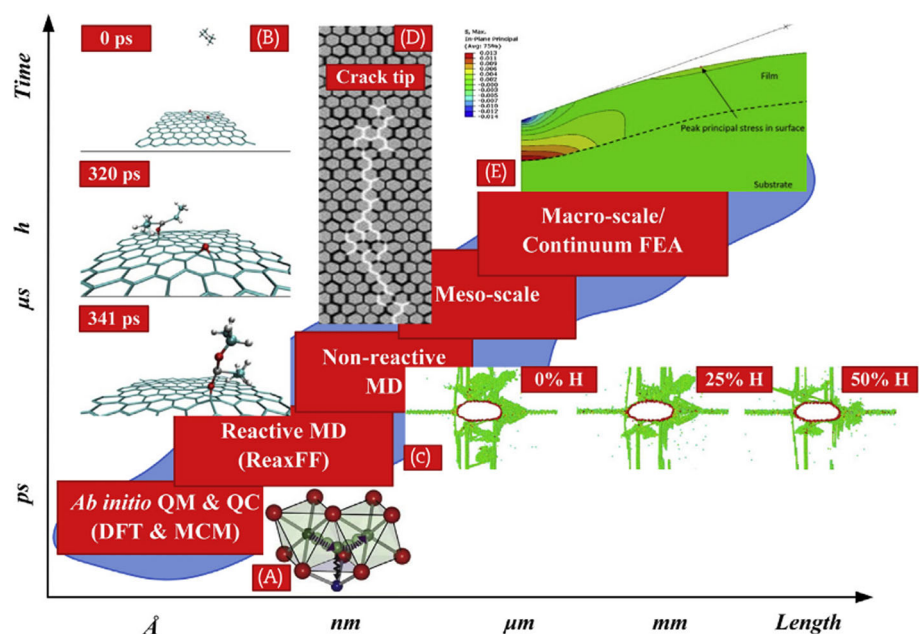
the SCC process spans atomic level (atomic bond cleavage), nanolevel (nanoscale crack nucleation), microlevel (nanoscale crack propagation into microscale crack) and macroscale crack visible to the naked eye [116–119]. The multiscale mechanical framework model is shown in Fig. 11. Only by carrying out multiscale correlation research and revealing the mechanism of the generation and development of material defects at different levels, the mechanism of SCC of materials can be clarified, which is not only of great theoretical significance, but also of great importance to the design and development of materials. It is also very important to improve the safety and reliability of materials service.

In recent years, multiscale methods have been considered to be an important way to solve engineering problems by scientific means and developed rapidly. In fact, fracture physics research based on MD and fracture mechanics research based on continuum mechanics have developed independently for many years and a lot of research results have been achieved. For simple structural fracture studies, the direct combination of computational MD and FEM has also achieved good results [120, 121], but the SCC with multiple factors is relatively more complex. It is necessary to study the different stages of SCC using different scales of calculation methods and also to explore the coupling relationship between different scales.

Das et al. [122] carried out a multiscale modeling study on the crack tip initial stage oxidation of Ni–Cr binary alloy for LWR structural material. SCC is characterized by localized and accelerated oxidation, and atomic methods based on quantum mechanics should be combined with continuum mechanics. Therefore, FEM analyses were applied to study the stress intensity effect on the CT specimen crack tip, and a 2- $\mu\text{m}$  rectangular region was prepared for the quasi-continuum (QC) model. The displacement load calculated by FEM was applied to the upper and lower boundaries of the QC model. Considering the atomic position of the deformed crystal structure, the water molecules were placed on the surface for quantum chemical molecular dynamics (QCMD) analysis, and the crack tip region from FEM to QCMD is shown in Fig. 12. It is known from the model that the early-stage surface oxidation process can certainly be influenced by SIF. Das et al. [123–125] also studied the crack tip early oxidation of Ni–Cr binary alloy based on DFT and QCMD. Wei et al. [126] studied the effect of hydrogen on intergranular crack evolution using first-principles and multiscale methods of viscous finite element and pointed out that it is very effective for studying the evolution of hydrogen-induced intergranular cracks.

The multiscale method provides a more systematic explanation for the micromechanism of SCC, but it is currently limited to the initial stage of oxidation and the stage of crack initiation. The treatment of

**Figure 11** Conceptual framework of multiscale mechanics model [119].



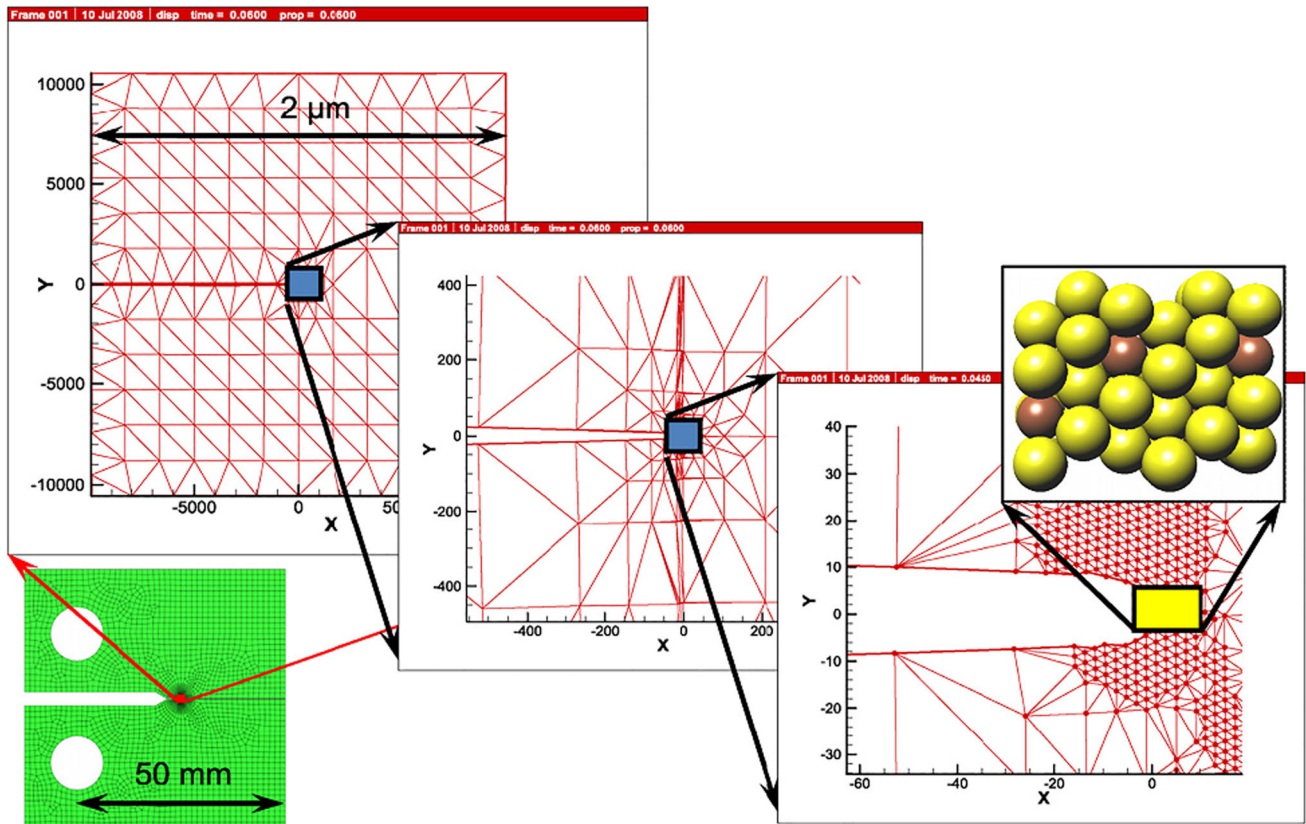


**Figure 12** Illustration of the crack tip region from FEM to QCMD [116].

temperature and timescales is not ideal, and a specific SCC growth rate model has not yet been formed, but it provides a powerful foundation and guidance.

## Conclusion and prospect

The establishment of SCC growth rates model can guarantee the safe, efficient and economic operation of the nuclear power plant. This paper summarizes the development of the three main methods for the prediction of SCC growth rates, i.e., empirical, deterministic and calculation methods.

1. Empirical models have evolved from traditional statistical analytical method to current ANN prediction method. At present, statistical analytical methods are gradually infiltrated with the mechanism of SCC, and the influence variables of CGR established by statistical analysis are gradually increasing. Now, statistical analysis methods have integrated more than ten influence variables, and the model has established relatively accurate parameters, which have been

applied to the actual service environment prediction of nuclear power materials. The development direction of MRP model will continuously improve the quantity and accuracy of CGR parameters. Currently, CGR empirical models include traditional statistical analysis methods, gray model and ANNs, but in the future more mathematical statistical methods will be applied to nuclear power material prediction. With the improvement and classification of the SCC experimental database of nuclear power materials, the empirical models are convenient and accurate and will continue to develop into an indispensable prediction model. For the complex system of SCC, empirical models can establish nonlinear relationship between multiple parameters. Particularly for the ANN model of artificial intelligence, it can make accurate prediction by learning existing data and comprehensively predict the influence of each factor on SCC. Through sensitivity analysis, the corresponding SCC mechanism is further explored, and the prediction range can exceed the scope covered by

experimental data, and its prediction results can enable people to study a complex problem more deeply.

2. Deterministic models must be based on the SCC mechanism, which includes how the various variables in the model interact and restrict each other, and the process of interaction and limitation itself is the law of nature. SCC is a very complicated process that involves a combination of materials, environment and stress. Experimental evidence and theoretical basis show that a single mechanism cannot explain the whole stress corrosion process, and the generation of a new mechanism is a process of continuous development and rejection. Accurate deterministic SCC growth rate model will continue to be the direction of future exploration, as deterministic prediction models are the embodiment of the highest level of predictive science and technology. The deterministic models based on SCC mechanism, such as slip-oxidation model, crack tip strain rate model, CEFM and SMM, developed vigorously at the end of last century. In the past ten years, it has been mainly improved on the basis of previous models, with a wider range of predictions. Of course, the revision and perfection will be a long-term process. However, the current SCC growth rate quantitative models are mainly based on the plane strain, and the future SCC model in the actual three-dimensional pipelines of nuclear power plants will be the key breakthrough direction. In addition, the critical SIF of SCC is also an important parameter for the study of stress corrosion, which is of great value for the establishment of relevant research models. With the deepening of theoretical research on HIC in recent years, more and more researchers pay attention to the role of hydrogen atoms in cracks and consider establishing CGR model with HIC as the main line, which is also the development direction of quantitative prediction model in the future. However, the deterministic model of perfect design does not exist, because all models are things we imagine fiction, and this fictional process itself has our imperfections of perception and wisdom.
3. Under the interaction of cross-scale, cross-time and multiple environmental factors, the related theories and experimental methods of service behavior and safety assessment of engineering

materials and structures are the key subjects at present. Calculation and simulation models achieve cross-scale computation from atomic scale to macroscale by FEM method based on fracture mechanics and multiscale method based on quantum mechanics and reveal the mechanism of crack initiation and propagation at different scales. By combining the FEM model based on fracture mechanics with the quantitative model of SCC, some concrete calculation models have been preliminarily formed. Multiscale method based on quantum mechanics has made great progress in the initial oxidation stage and crack initiation stage, but no concrete crack propagation model has been formed. It will be the future direction of calculation and simulation to establish the correlation between crack propagation and time domain. Calculation and simulation provide a new idea and tool for the study of SCC mechanism in the future and lay a strong foundation for the study of SCC growth rate, which have become the third way to discover new concepts and mechanisms after experiments and theories.

## Acknowledgements

The authors acknowledge the financial supports from the Beijing Municipal Science & Technology Commission (Z181100005218005).

## References

- [1] Andresen PL (2019) A brief history of environmental cracking in Hot Water. *Corrosion* 75(3):240–253
- [2] Wang M, Song M, Lear CR, Was GS (2019) Irradiation assisted stress corrosion cracking of commercial and advanced alloys for light water reactor core internals. *J Nucl Mater* 515:52–70
- [3] Ashour EA (2001) Crack growth rates of Inconel 600 in aqueous solutions at elevated temperature. *J Mater Sci* 36(3):685–692. <https://doi.org/10.1023/A:1004884823922>
- [4] Chen K, Wang J, Du D, Andresen PL, Zhang L (2018) dK/da effects on the SCC growth rates of nickel base alloys in high-temperature water. *J Nucl Mater* 503:13–21
- [5] Shen Z, Meisner M, Arika K, Lozano-Perez S (2019) Mechanistic understanding of the temperature dependence of crack growth rate in alloy 600 and 316 stainless steel

- through high-resolution characterization. *Acta Mater* 165:73–86
- [6] Rebak RB, Szklarska-Smialowska Z (1996) The mechanism of stress corrosion cracking of alloy 600 in high temperature water. *Corros Sci* 38(6):971–988
- [7] Saito K, Kuniya J (2001) Mechanochemical model to predict stress corrosion crack growth of stainless steel in high temperature water. *Corros Sci* 43(9):1751–1766
- [8] Hall MM (2009) Film rupture model for aqueous stress corrosion cracking under constant and variable stress intensity factor. *Corros Sci* 51(2):225–233
- [9] Turnbull A, Wright L (2017) Modelling the electrochemical crack size effect on stress corrosion crack growth rate. *Corros Sci* 126:69–77
- [10] Fekete B, Ai J, Yang J, Han JS, Maeng WY, Macdonald DD (2018) An advanced coupled environment fracture model for hydrogen-induced cracking in alloy 600 in PWR primary heat transport environment. *Theor Appl Fract Mech* 95:233–241
- [11] Du D, Chen K, Yu L, Yu H, Lu H, Zhang L, Shi X, Xu X (2015) SCC crack growth rate of cold worked 316L stainless steel in PWR environment. *J Nucl Mater* 456:228–234
- [12] Lim YS, Kim DJ, Kim SW, Kim HP (2019) Crack growth and cracking behavior of Alloy 600/182 and Alloy 690/152 welds in simulated PWR primary water. *Nucl Eng Technol* 51(1):228–237
- [13] Materials Reliability Program (2002) Crack growth rates for evaluating primary water stress corrosion cracking (PWSCC) of thick-wall alloy 600 materials (MRP-55), EPRI, Palo Alto, CA: 1006695
- [14] White GA, Hickling J, Mathews LK (2003) Crack growth rates for evaluating PWSCC of thick-wall alloy 600 material. In: Proceedings of the 11th international conference environmental degradation materials nuclear power systems-water reactors, ANS, pp 166–179
- [15] Materials Reliability Program (2004) Crack growth rates for evaluating primary water stress corrosion cracking (PWSCC) of alloy 82, 182, and 132 welds (MRP-115), EPRI, Palo Alto, CA:1006696
- [16] White GA, Nordmann NS, Hickling J, Harrington CD (2005) Development of crack growth rate disposition curves for primary water stress corrosion cracking (PWSCC) of Alloy 82, 182, and 132 Weldments. In: Proceedings of 12th international conference environmental degradation materials nuclear power systems-water reactors, TMS, pp 511–530
- [17] Lu Z, Shoji T, Xue H, Fu C (2013) Deterministic formulation of the effect of stress intensity factor on PWSCC of Ni-base alloys and weld metals. *J Pressure Vess-T ASME* 135(2):021402-021402-9. <https://doi.org/10.1115/1.4007471>
- [18] Materials Reliability Program (2017) Crack growth rates for PWSCC of alloy 690 and alloy 52, 152, and variants welds (MRP-386), EPRI, Palo Alto, CA:3002010756
- [19] Materials Reliability Program (2017) Crack growth rates for evaluating PWSCC of alloy 600 materials and alloy 82, 182, and 132 welds (MRP-420), EPRI Palo Alto, CA:3002010758
- [20] Scott PM (1991) An analysis of primary water stress corrosion cracking in PWR steam generators. In: Proceedings of the specialists meeting on operating experience with steam generators, Brussels, Belgium, pp 5–6
- [21] Jenks AR, White GA, Crooker P (2017) Crack growth rates for evaluating PWSCC of thick-wall alloy 690 material and alloy 52, 152, and variant welds. In: ASME. Pressure vessels and piping conference, volume 6B: materials and fabrication: V06BT06A012. <https://doi.org/10.1115/pv2017-65886>
- [22] Smets HMG, Bogaerts WFL (1992) SCC analysis of austenitic stainless steels in chloride-bearing water by neural network techniques. *Corrosion* 48(8):618–623
- [23] Lu PC (1997) Using neural network techniques to predict crack growth rates of stress corrosion. *Int J Mater Prod Technol* 12:329–345
- [24] Kamrunnihar M, Urquidi-Macdonald M (2010) Prediction of corrosion behavior using neural network as a data mining tool. *Corros Sci* 52(3):669–677
- [25] Kamrunnihar M, Urquidi-Macdonald M (2011) Prediction of corrosion behaviour of Alloy 22 using neural network as a data mining tool. *Corros Sci* 53(3):961–967
- [26] Shi J, Wang J, Macdonald DD (2014) Prediction of crack growth rate in type 304 stainless steel using artificial neural networks and the coupled environment fracture model. *Corros Sci* 89:69–80
- [27] Shi J, Wang J, Macdonald DD (2015) Prediction of primary water stress corrosion crack growth rates in alloy 600 using artificial neural networks. *Corros Sci* 92:217–227
- [28] Halama M, Kreislova K, Lysebettens JV (2011) Prediction of atmospheric corrosion of carbon steel using artificial neural network model in local geographical regions. *Corrosion* 67(6):065004-1–065004-6. <https://doi.org/10.5006/1.3595099>
- [29] Li Y, Xu T, Wang S, Fekete B, Yang J, Yang J, Qiu J, Xu A, Wang J, Xu Y, Macdonald DD (2019) Modelling and analysis of the corrosion characteristics of ferritic-martensitic steels in supercritical water. *Materials*. <https://doi.org/10.3390/ma12030409>
- [30] Hu Q, Liu Y, Zhang T, Geng S, Wang F (2019) Modeling the corrosion behavior of Ni–Cr–Mo–V high strength steel

- in the simulated deep sea environments using design of experiment and artificial neural network. *J Mater Sci Technol* 35(1):168–175
- [31] Lin YC, Fang X, Wang YP (2008) Prediction of metadynamic softening in a multi-pass hot deformed low alloy steel using artificial neural network. *J Mater Sci* 43(16):5508–5515. <https://doi.org/10.1007/s10853-008-2832-6>
- [32] Malho Rodrigues A, Franceschi S, Perez E, Garrigues JC (2015) Formulation optimization for thermoplastic sizing polyetherimide dispersion by quantitative structure-property relationship: experiments and artificial neural networks. *J Mater Sci* 50(1):420–426. <https://doi.org/10.1007/s10853-014-8601-9>
- [33] Shah M, Das SK (2018) An artificial neural network model to predict the Bainite plate thickness of nanostructured Bainitic steels using an efficient Network-Learning Algorithm. *J Mater Eng Perform* 27(11):5845–5855
- [34] Sontag ED (1992) Feedback stabilization using two-hidden-layer nets. *IEEE Trans Neural Netw* 3(6):981–990
- [35] Srinivasan S, Saghir MZ (2013) Modeling of thermo-transport phenomenon in metal alloys using artificial neural networks. *Appl Math Model* 37(5):2850–2869
- [36] Lin Y, Cunningham GA (1995) A new approach to fuzzy-neural system modeling. *IEEE Trans Fuzzy Syst* 3(2):190–198
- [37] Ham FM, Kostanic I (2000) Principles of neurocomputing for science and engineering, 1st edn. McGraw-Hill, New York
- [38] Coskun MI, Karahan IH (2018) Modeling corrosion performance of the hydroxyapatite coated CoCrMo biomaterial alloys. *J Alloys Comput* 745:840–848
- [39] Cottis RA, Li Q, Owen G, Gartland SJ, Helliwell IA, Turega M (1999) Neural network methods for corrosion data reduction. *Mater Des* 20(4):169–178
- [40] Kumar G, Buchheit RG (2012) Use of artificial neural network models to predict coated component life from short-term electrochemical impedance spectroscopy measurements. *Corrosion* 64(3):241–254
- [41] Cavanaugh MK, Buchheit RG, Birbilis N (2010) Modeling the environmental dependence of pit growth using neural network approaches. *Corros Sci* 52(9):3070–3077
- [42] Ford FP, Emigh PW (1985) The prediction of the maximum corrosion fatigue crack propagation rate in the low alloy steel-de-oxygenated water system at 288°C. *Corros Sci* 25(8):673–692
- [43] Andresen PL, Ford FP (1988) Life prediction by mechanistic modeling and system monitoring of environmental cracking of iron and nickel alloys in aqueous systems. *Mater Sci Eng A* 103(1):167–184
- [44] Logan HL (1952) Film-rupture mechanism of stress corrosion. *J Res Natl Bur Stand* 48:99–105
- [45] Woodtli J, Kieselbach R (2000) Damage due to hydrogen embrittlement and stress corrosion cracking. *Eng Fail Anal* 7(6):427–450
- [46] Scully JC (1968) The mechanical parameters of stress-corrosion cracking. *Corros Sci* 8(10):759–769
- [47] Vermilyea DA (1972) A theory for the propagation of stress corrosion cracks in metals. *J Electrochem Soc* 119(4):405–407
- [48] Parkins RN (1980) Predictive approaches to stress corrosion cracking failure. *Corros Sci* 20(2):147–166
- [49] Parkins RN (1987) Current topics in corrosion: factors influencing stress corrosion crack growth kinetics. *Corrosion* 43(3):130–139
- [50] Ford FP (1996) Quantitative prediction of environmentally assisted cracking. *Corrosion* 52:375–395
- [51] Andresen PL (1988) Environmentally assisted growth rate response of nonsensitized AISI 316 grade stainless steels in high temperature water. *Corrosion* 44(7):450–460
- [52] Ford FP (1988) Status of research on environmentally assisted cracking in LWR pressure vessel steels. *J Press Vess-T ASME* 110(2):113–128
- [53] Andresen PL, Ford FP (1993) Use of fundamental modeling of environmental cracking for improved design and lifetime evaluation. *J Press Vess-T ASME* 115(4):353–358
- [54] Andresen PL, Ford FP (1994) Fundamental modeling of environmental cracking for improved design and lifetime evaluation in BWRs. *Int J Press Vessel Pip* 59(1–3):61–70
- [55] Shoji T, Lu Z, Murakami H (2010) Formulating stress corrosion cracking growth rates by combination of crack tip mechanics and crack tip oxidation kinetics. *Corros Sci* 52(3):769–779
- [56] Macdonald DD (1996) On the modeling of stress corrosion cracking in iron and nickel base alloys in high temperature aqueous environments. *Corros Sci* 38(6):1003–1010
- [57] Gutman EM (2007) An inconsistency in “film rupture model” of stress corrosion cracking. *Corros Sci* 49(5):2289–2302
- [58] Hall MM (2009) Critique of the Ford–Andresen film rupture model for aqueous stress corrosion cracking. *Corros Sci* 51(5):1103–1106
- [59] Ford FP, Taylor DF, Andresen PL, Ballinger RG (1987) Corrosion-assisted cracking of stainless and low alloy steels in LWR environments. In: EPRI final report RP2006-6, Electric Power Research Institute
- [60] Rice JR, Sorensen EP (1978) Continuing crack-tip deformation and fracture for plane-strain crack growth in elastic-plastic solids. *J Mech Phys Solids* 26(3):163–186

- [61] Rice JR, Drugan WJ, Sham TL (1980) Elastic–plastic analysis of growing cracks. In: Proceedings of the 12th national symposium on fracture mechanics. ASTM Special Technical Publication, Philadelphia, pp 189–221
- [62] Congleton J, Shoji T, Parkins RN (1985) The stress corrosion cracking of reactor pressure vessel steel in high temperature water. *Corros Sci* 25(8):633–650
- [63] Shoji T, Suzuki S, Ballinger RG (1995) Theoretical prediction of SCC growth behavior-threshold and plateau growth rate. In: Proceedings of the seventh international symposium on environmental degradation of materials in nuclear power systems, Breckinridge, pp 881–889
- [64] Peng QJ, Kwon J, Shoji T (2004) Development of a fundamental crack tip strain rate equation and its application to quantitative prediction of stress corrosion cracking of stainless steels in high temperature oxygenated water. *J Nucl Mater* 324:52–61
- [65] Hutchinson JW (1968) Plastic stress and strain fields at a crack tip. *J Mech Phys Solids* 16(5):337–342
- [66] Rice JR, Rosengren GF (1968) Plane strain deformation near a crack tip in a power-law hardening material. *J Mech Phys Solids* 16(1):1–12
- [67] Gao Y, Hwang K (1981) Elastic plastic fields in steady crack growth in a strain hardening material. *Geochem Int* 50(50):330–343
- [68] Gao Y, Zhang X, Hwang K (1983) The asymptotic near-tip solution for mode-III crack in steady growth in power hardening media. *Int J Fract* 21(4):301–317
- [69] Gerberich W, Davidson DL, Kaczorowski M (1990) Experimental and theoretical strain distributions for stationary and growing cracks. *J Mech Phys Solids* 38(1):87–113
- [70] Fan TY, Sutton MA, Zhang LX (1997) Plane stress steady crack growth in a power-law hardening material. *Int J Fract* 86(4):327–341
- [71] Hall M (2008) An alternative to the Shoji crack tip strain rate equation. *Corros Sci* 50(10):2902–2905
- [72] Koshiishi M, Hashimoto T, Obata R (2017) Application of the FRI crack growth model for neutron-irradiated stainless steels in high-temperature water of a boiling water reactor environment. *Corros Sci* 123:178–288
- [73] MacDonald DD, Urquidi-MacDonald M (1991) A coupled environment model for stress corrosion cracking in sensitized type 304 stainless steel in LWR environments. *Corros Sci* 32:51–81
- [74] Macdonald DD, Lu PC, Urquidi-Macdonald M, Yeh TK (1996) Theoretical estimation of crack growth rates in type 304 stainless steel in boiling-water reactor coolant environments. *Corrosion* 52(10):768–785
- [75] Vankeerberghen M, Macdonald DD (2002) Predicting crack growth rate vs. temperature behaviour of type 304 stainless steel in dilute sulphuric acid solutions. *Corros Sci* 44(7):1425–1441
- [76] Lee SK, Lv P, Macdonald DD (2013) Customization of the CEFM for predicting stress corrosion cracking in lightly sensitized Al-Mg alloys in marine applications. *J Solid State Electrochem* 17(8):2319–2332
- [77] Liu S, Macdonald DD (2002) Fracture of AISI 4340 steel in concentrated sodium hydroxide solution. *Corrosion* 58(10):835–845
- [78] Maeng WY, Macdonald DD (2008) The effect of acetic acid on the stress corrosion cracking of 3.5NiCrMoV turbine steels in high temperature water. *Corros Sci* 50(8):2239–2250
- [79] Shi J, Fekete B, Wang J, Macdonald DD (2018) Customization of the coupled environment fracture model for predicting stress corrosion cracking in Alloy 600 in PWR environment. *Corros Sci* 139:58–67
- [80] Engelhardt GR, Urquidi-Macdonald M, Macdonald DD (1997) A simplified method for estimating corrosion cavity growth rates. *Corros Sci* 39(3):419–441
- [81] Engelhardt GR, Macdonald DD (2010) Modelling the crack propagation rate for corrosion fatigue at high frequency of applied stress. *Corros Sci* 52(4):1115–1122
- [82] Engelhardt GR, Macdonald DD, Millett PJ (1999) Transport processes in steam generator crevices-I. General corrosion model. *Corros Sci* 41(11):2165–2190
- [83] Engelhardt GR, Macdonald DD, Millett PJ (1999) Transport processes in steam generator crevices. II. A simplified method for estimating impurity accumulation rates. *Corros Sci* 41(11):2191–2211
- [84] Lee SK, Kramer D, Macdonald DD (2014) On the shape of stress corrosion cracks in sensitized type 304 SS in Boiling Water Reactor primary coolant piping at 288°C. *J Nucl Mater* 454(1–3):359–372
- [85] Macdonald DD (1981) Redox potential measurements in high temperature aqueous systems. *J Electrochem Soc* 128(2):250–257
- [86] Andresen PL, Ford FP (1996) Response to “On the modeling of stress corrosion cracking of iron and nickel base alloys in high temperature aqueous environments”. *Corros Sci* 38(6):1011–1016
- [87] Macdonald DD (1997) Clarification of issues raised by P.L. Andresen and F.P. Ford in their response to “On the modeling of stress corrosion cracking of iron and nickel base alloys in high temperature aqueous environments”. *Corros Sci* 39(8):1487–1490

- [88] Galvele JR (1986) Enhanced surface mobility as the cause of stress corrosion cracking. *J Electrochem Soc* 113:953–954
- [89] Galvele JR (1987) A stress corrosion cracking mechanism based on surface mobility. *Corros Sci* 27(1):1–33
- [90] Galvele JR (1993) Surface mobility mechanism of stress-corrosion cracking. *Corros Sci* 35(1):419–434
- [91] Galvele JR (1996) Application of the surface-mobility stress corrosion cracking mechanism to nuclear materials. *J Nucl Mater* 229:139–148
- [92] Galvele JR (2000) Recent developments in the surface-mobility stress-corrosion-cracking mechanism. *Electrochim Acta* 45(21):3537–3541
- [93] Galvele JR (2004) Reply to E.M. Gutman's: "Comments on the "Stress corrosion cracking of zirconium and zircaloy-4 in halide aqueous solutions" by S.B. Farina, G.S. Duffo, J.R. Galvele". *Corros Sci* 46(7):1807–1812
- [94] Sieradzki K, Friedersdorf FJ (1994) Notes on the surface mobility mechanism of stress-corrosion cracking. *Corros Sci* 36(4):669–675
- [95] Galvele JR (1994) Comments on "notes on the surface mobility mechanism of stress-corrosion cracking", by K. Sieradzki and F. J. Friedersdorf. *Corros Sci* 36(5):901–910
- [96] Gutman EM (2004) Comments on the "Stress corrosion cracking of zirconium and zircaloy-4 in halide aqueous solutions" by S.B. Farina, G.S. Duffo, J.R. Galvele. *Corros Sci* 46(7):1801–1806
- [97] Zhu X, Zi G (2017) A 2D mechano-chemical model for the simulation of reinforcement corrosion and concrete damage. *Constr Build Mater* 137:330–344
- [98] Satoh T, Nakazato T, Moriya S, Suzuki S, Shoji T (1998) Quantitative prediction of environmentally assisted cracking based on a theoretical model and computer simulation. *J Nucl Mater* 258–263(4):2054–2058
- [99] Xue H, Shoji T (2007) Quantitative prediction of EAC crack growth rate of sensitized type 304 stainless steel in boiling water reactor environments based on EPFEM. *J Press Vess-T ASME* 129(3):460–467
- [100] Xue H, Sato Y, Shoji T (2009) Quantitative estimation of the growth of environmentally assisted cracks at flaws in light water reactor components. *J Press Vess-T ASME* 131(1):011404-1–011404-9
- [101] Xue H, Li Z, Lu Z, Shoji T (2011) The effect of a single tensile overload on stress corrosion cracking growth of stainless steel in a light water reactor environment. *Nucl Eng Des* 241(3):731–738
- [102] Yang F, Xue H, Zhao L, Fang X (2014) Effects of stress intensity factor on electrochemical corrosion potential at crack tip of nickel-based alloys in high temperature water environments. *Rare Metal Mat Eng* 43(3):513–518
- [103] Xue H, Li Y (2016) Micro-mechanical state at tip of environmentally assisted cracking in nickel-based alloy. *Rare Metal Mat Eng* 45(3):537–541
- [104] Yang F, Xue H, Zhao L, Fang X (2016) Influence of nickel-based alloys' mechanical properties on mechanochemical effect at crack tip in high temperature water environments. *Rare Metal Mat Eng* 45(7):1641–1646
- [105] Zhao L, Cui Y, Yang F, Xue H (2018) Analysis on crack driving force at stress corrosion cracking tip induced by scratch in nickel-based alloy. *Rare Metal Mat Eng* 47(5):1399–1405
- [106] Jivkov AP, Stahle P (2002) Strain-driven corrosion crack growth: a pilot study of intergranular stress corrosion cracking. *Eng Fract Mech* 69(18):2095–2111
- [107] Jivkov AP (2002) Strain-assisted corrosion cracking and growth rate inhibitors. Ph.D. Dissertation, Malmö University
- [108] Jivkov AP (2004) Strain-induced passivity breakdown in corrosion crack initiation. *Theor Appl Fract Mec* 42:43–52
- [109] Jivkov AP (2003) Evolution of fatigue crack corrosion from surface irregularities. *Theor Appl Fract Mec* 40(1):45–54
- [110] Jivkov AP, Stevens NPC, Marrow TJ (2006) A two-dimensional mesoscale model for intergranular stress corrosion crack propagation. *Acta Mater* 54(13):3493–3501
- [111] Jivkov AP, Stevens NPC, Marrow TJ (2006) A three-dimensional computational model for intergranular cracking. *Comput Mater Sci* 38(2):442–453
- [112] Belytschko T, Black T (1999) Elastic crack growth in finite elements with minimal remeshing. *Inter J Numer Math Eng* 45(5):601–620
- [113] Lee SJ, Chang YS (2015) Evaluation of primary water stress corrosion cracking growth rates by using the extended finite element method. *Nucl Eng Technol* 47(7):895–906
- [114] Lee H, Kang SJ, Choi JB, Kim MK (2017) An extended finite element method-based representative model for primary water stress corrosion cracking of a control rod driving mechanism penetration nozzle. *Fatigue Fract Eng Mater Struct* 41(1):1–8
- [115] Kang SJ, Lee H, Choi JB, Kim MK (2017) PWSCC initiation and propagation in a CRDM penetration nozzle. *J Mech Sci Technol* 31(11):5387–5395
- [116] Saxena S, Ramakrishnan N (2007) A comparison of micro, meso and macroscale FEM analysis of ductile fracture in a CT specimen (mode I). *Comput Mater Sci* 39(1):1–7
- [117] Ersland CH, Thaulow C, Vatne IR, Østby E (2012) Atomistic modeling of micromechanisms and T-stress effects in fracture of iron. *Eng Fract Mech* 79:180–190
- [118] Bitzek E, Kermode JR, Gumbsch P (2015) Atomistic aspects of fracture. *Int J Fract* 191(1–2):13–30



- [119] Liu X, Hwang W, Park J, Van D, Chang Y, Lee SH, Kim S-Y, Han S, Lee B (2018) Towards the multiscale nature of stress corrosion cracking. *Nucl Eng Technol* 50(1):1–17
- [120] Xiao SP, Belytschko T (2004) A bridging domain method for coupling continua with molecular dynamics. *Comput Method Appl M* 193(17–20):1645–1669
- [121] Xu T, Stewart R, Fan J, Zeng X, Yao A (2016) Bridging crack propagation at the atomistic and mesoscopic scale for BCC-Fe with hybrid multiscale methods. *Eng Fract Mech* 155:166–182
- [122] Das NK, Tirtom I, Shoji T (2010) A multiscale modelling study of Ni–Cr crack tip initial stage oxidation at different stress intensities. *Mater Chem Phys* 122(2–3):336–342
- [123] Das NK, Suzuki K, Takeda Y, Ogawa K, Shoji T (2008) Quantum chemical molecular dynamics study of stress corrosion cracking behavior for fcc Fe and Fe-Cr surfaces. *Corros Sci* 50(6):1701–1706
- [124] Das NK, Shoji T (2011) A density functional study of atomic oxygen and water molecule adsorption on Ni (111) and chromium-substituted Ni (111) surfaces. *Appl Surf Sci* 258(1):442–447
- [125] Das NK, Shoji T (2013) Early stage oxidation of Ni-Cr binary alloy (111), (110) and (100) surfaces: a combined density functional and quantum chemical molecular dynamics study. *Corros Sci* 73:18–31
- [126] Wei X, Dong C, Chen Z, Xiao K, Li X (2016) The effect of hydrogen on the evolution of intergranular cracking: a cross-scale study using first-principles and cohesive finite element methods. *RSC Adv* 6(33):27282–27292

**Publisher's Note** Springer Nature remains neutral with regard to jurisdictional claims in published maps and institutional affiliations.